Gut cytokines modulate olfaction through metabolic reprogramming of glia

https://doi.org/10.1038/s41586-021-03756-0

Received: 13 October 2020

Accepted: 22 June 2021

Published online: 21 July 2021

Check for updates

Xiaoyu Tracy Cai[1,2,3], Hongjie Li[4,5,6], Martin Borch Jensen[2,7], Elie Maksoud[2], Jovencio Borneo[8], Yuxin Liang[9], Stephen R. Quake[10,11], Liqun Luo[4], Pejmun Haghighi[2] & Heinrich Jasper[1,2]✉

Infection-induced aversion against enteropathogens is a conserved sickness behaviour that can promote host survival[1,2]. The aetiology of this behaviour remains poorly understood, but studies in *Drosophila* have linked olfactory and gustatory perception to avoidance behaviours against toxic microorganisms[3–5]. Whether and how enteric infections directly influence sensory perception to induce or modulate such behaviours remains unknown. Here we show that enteropathogen infection in *Drosophila* can modulate olfaction through metabolic reprogramming of ensheathing glia of the antennal lobe. Infection-induced unpaired cytokine expression in the intestine activates JAK–STAT signalling in ensheathing glia, inducing the expression of glial monocarboxylate transporters and the apolipoprotein *glial lazarillo* (*GLaz*), and affecting metabolic coupling of glia and neurons at the antennal lobe. This modulates olfactory discrimination, promotes the avoidance of bacteria-laced food and increases fly survival. Although transient in young flies, gut-induced metabolic reprogramming of ensheathing glia becomes constitutive in old flies owing to age-related intestinal inflammation, which contributes to an age-related decline in olfactory discrimination. Our findings identify adaptive glial metabolic reprogramming by gut-derived cytokines as a mechanism that causes lasting changes in a sensory system in ageing flies.

Olfactory perception influences nutrition and promotes physiological and mental well-being[6,7]. In flies, a dedicated olfactory circuit elicits avoidance behaviours towards geosmin—a volatile compound that is released by mould and some bacteria[4]. Olfactory receptors also mediate an initial attraction to food that contains certain enteropathogens[3,5]. After infection with these pathogens, however, an avoidance behaviour is triggered by immune receptors in the brain[3], gustatory bitter neurons, and the neuropeptide leukokinin[5]. Whether changes in olfactory perception contribute to this behavioural switch from attraction to avoidance remains unclear.

In *Drosophila*, odorants are sensed by olfactory receptor neurons in the head, the antenna and the maxillary palp. Olfactory receptor neurons synapse into projection neurons at the antennal lobe (AL), where the signal is converted into a spatiotemporal code in 50 glomerular compartments[8]. Projection neurons axons project to higher olfactory centres to instruct innate and learned behaviour. In this system, glia and neurons operate as a tightly coupled unit to maintain olfactory sensitivity[9,10].

In ageing flies, olfactory perception of both aversive and attractive odours declines[11], but the mechanism(s) of this decline remain unclear. Olfactory perception and other neurological processes also decline in ageing mammals, often influenced by gastrointestinal signals[12,13].

Here, we investigate the communication between the gut and the brain, and how it influences infection-induced avoidance behaviour, infection tolerance, and olfactory decline during ageing.

Enteric infection modulates olfaction

We used a modified capillary feeder (CAFE) assay to measure choice between food that did or did not contain *Erwinia carotovora carotovora 15* (*Ecc15*), a non-lethal enteropathogen that causes intestinal inflammation[14] (Extended Data Fig. 1a). Consistent with recent reports[3], naive flies consumed more *Ecc15*-containing food than normal food (Fig. 1a). However, when orally infected with *Ecc15* for 24 h before the feeding assay, flies developed a distinct aversion to food that contained *Ecc15* (Fig. 1a, Extended Data Fig. 1b). To assess whether this involved changes in olfactory perception, we determined the 'preference index' for attractive (such as putrescine[11]) or aversive (such as 3-octanol[11]) odours in T-maze assays[11] (Extended Data Fig. 1c). Preference or aversion for attractive or aversive odours, respectively, declined after infection, which indicates that infection causes a non-selective decline in olfactory discrimination (Fig. 1b, Extended Data Fig. 1d). This was transient, as olfactory discrimination recovered 5 days after infection (Fig. 1b, Extended Data Fig. 1d), coincident with the clearance of bacteria and epithelial regeneration in the intestine[15]. Olfactory discrimination was

[1]Immunology Discovery, Genentech, Inc., South San Francisco, CA, USA. [2]Buck Institute for Research on Aging, Novato, CA, USA. [3]University of Southern California, Los Angeles, CA, USA. [4]Department of Biology and Howard Hughes Medical Institute, Stanford University, Stanford, CA, USA. [5]Huffington Center on Aging, Baylor College of Medicine, Houston, TX, USA. [6]Department of Molecular and Human Genetics, Baylor College of Medicine, Houston, TX, USA. [7]Gordian Biotechnology, San Francisco, CA, USA. [8]FACS lab, Genentech, Inc., South San Francisco, CA, USA. [9]NGS lab, Genentech, Inc., 1 DNA Way, South San Francisco, CA, USA. [10]Department of Bioengineering and Department of Applied Physics, Stanford University, Stanford, CA, USA. [11]Chan Zuckerberg Biohub, Stanford, CA, USA. ✉e-mail: jasperh@gene.com

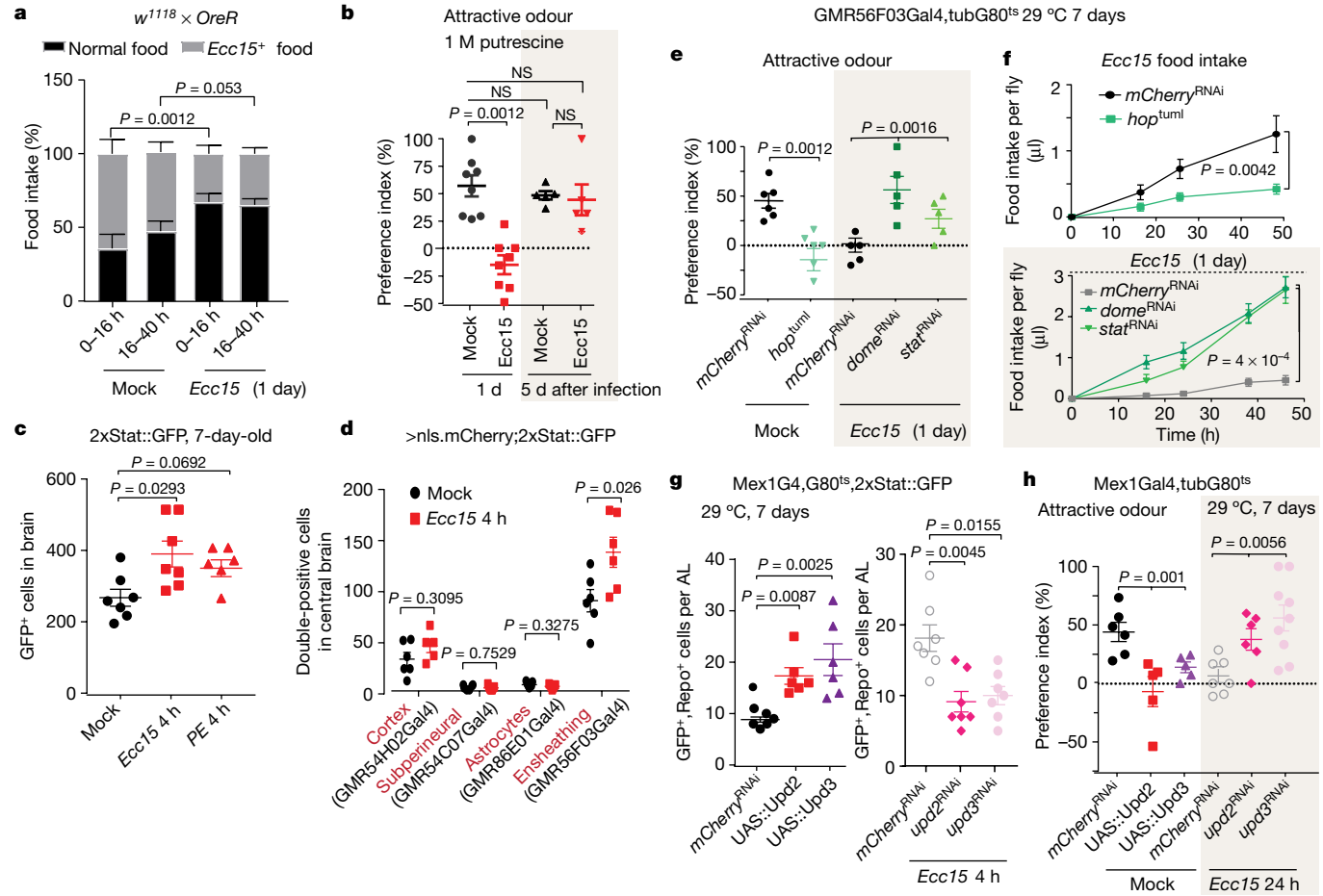

Fig. 1 | JAK–STAT signalling in EG after infection transiently inhibits olfactory discrimination, contributing to *Ecc15* aversion, and host survival. a, Food preference (normal food or *Ecc15*$^+$ food) of wild-type flies with or without *Ecc15* infection. **b**, Olfactory perception of young flies 24 h (1 d) and 5 days (5 d) after *Ecc15* infection., as measured by preference index towards putrescine. **c**, Numbers of STAT::GFP$^+$ cells in the central brains from flies infected or not with *Ecc15* or *PE* for 4 h. Images are shown in Extended Data Fig. 1h; 48-µm *z*-sections were quantified per condition. **d**, STAT activity in each subtype of glia with or without *Ecc15* infection. **e**, Preference index of young flies towards 1 M putrescine with indicated JAK–STAT perturbation in EG. **f**, Intake of *Ecc15*$^+$ food by young flies with indicated JAK–STAT perturbation in EG. **g**, Numbers of STAT::GFP$^+$ glia per AL from young flies with indicated *upd2* or *upd3* perturbation in enterocytes. Images are shown in Extended Data Fig. 4c, 4d. **h**, Preference index of young flies towards 1 M putrescine with indicated perturbations of *upd2* or *upd3* in enterocytes. Data are mean and s.e.m. $n = 7$ replicates (3 flies per cohort) per condition in **a**, $n = 8, 8, 5$ and 5 independently performed experiments per condition (from left to right) in **b**, $n = 7, 7$ and 6 brains per condition (from left to right) in **c**, $n = 6, 5, 6, 7, 7, 7, 6$ and 6 brains per condition (from left to right) in **d**, $n = 6, 7, 5, 5$ and 5 independently performed experiments per condition (from left to right) in **e**, $n = 8$ and 9 replicates (3 flies per cohort) for *mCherry*^{RNAi} and *hop*^{tuml} in **f** (top), 6, 8 and 7 replicates for *mCherry*^{RNAi}, *dome*^{RNAi} and *stat*^{RNAi} in **f** (bottom). $n = 7, 6$ and 6 flies for *mCherry*^{RNAi}, UAS::Upd2 and UAS::Upd3 in **g** (left), $n = 7$ flies per condition in **g** (right), $n = 6, 5, 5, 7, 6$ and 9 independently performed experiments per condition (from left to right) in **h**. Data shown in **d** are representative of two independently performed experiments, and those shown in **a**, **c**, **f** and **g** are representative from three separate experiments. *P* values in **a**, **d**, **e** (left) and **f** (top) from two-tailed Mann–Whitney test; *P* values in **b**, **c** and **g** from Dunn's multiple comparisons test; other *P* values from Kruskal–Wallis test. NS, not significant ($P > 0.9999$ in **b**).

not influenced by starvation or exposure to heat-killed *Ecc15* (Extended Data Fig. 1e, f). Consistent with their reported role in sensing pathogenic bacteria[3,5], the CO_2 receptor Gr63a or the odorant receptor co-receptor Orco was required for the attraction to *Ecc15* food: *Orco*[1] and *Gr63a*[1] mutants ingested less *Ecc15* food under naive conditions, and when infected, failed to further reduce ingestion of *Ecc15*-containing food (Extended Data Fig. 1g). Together, these observations suggest that after an initial odorant-mediated attraction, flies develop aversion to enteropathogens, through a concerted activation of gustatory and immune receptors[3,5] and suppression of olfaction.

After oral infection with *Ecc15*, damaged intestinal enterocytes produce the inflammatory IL-6-like cytokines Unpaired 2 and 3 (Upd2 and Upd3) to stimulate intestinal stem-cell proliferation and epithelial regeneration[14]. Proteins of the Upd family activate the JAK–STAT signalling pathway through the receptor Domeless (Dome) and the JAK homologue Hopscotch (Hop). Using the 2xSTAT::GFP reporter for JAK–STAT pathway activity[16], we found upregulated GFP expression in the brain 4 h after oral *Ecc15* infection, as well as after oral infection with the more lethal enteropathogen *Pseudomonas entomophila* (*PE*) that damages the gut epithelium[15] (Fig. 1c, Extended Data Fig. 1h). JAK–STAT activity was observed in a sparse population of cells of the brain that stained positive for the glial marker Repo (Extended Data Fig. 1i). Subtype-specific Gal4 drivers revealed that among the five subtypes of *Drosophila* glia (astrocytes, ensheathing, perineural, subperineural and cortex glia[17]), ensheathing glia (EG) were the main population that upregulate STAT activity in response to *Ecc15* infection (Fig. 1d, Extended Data Fig. 2a). This was confirmed using four different Gal4 drivers to label EG (Extended Data Fig. 2b–d) and by flow cytometry (Extended Data Fig. 2e). Infection did not influence numbers (Extended Data Fig. 2c) and membranous processes (labelled

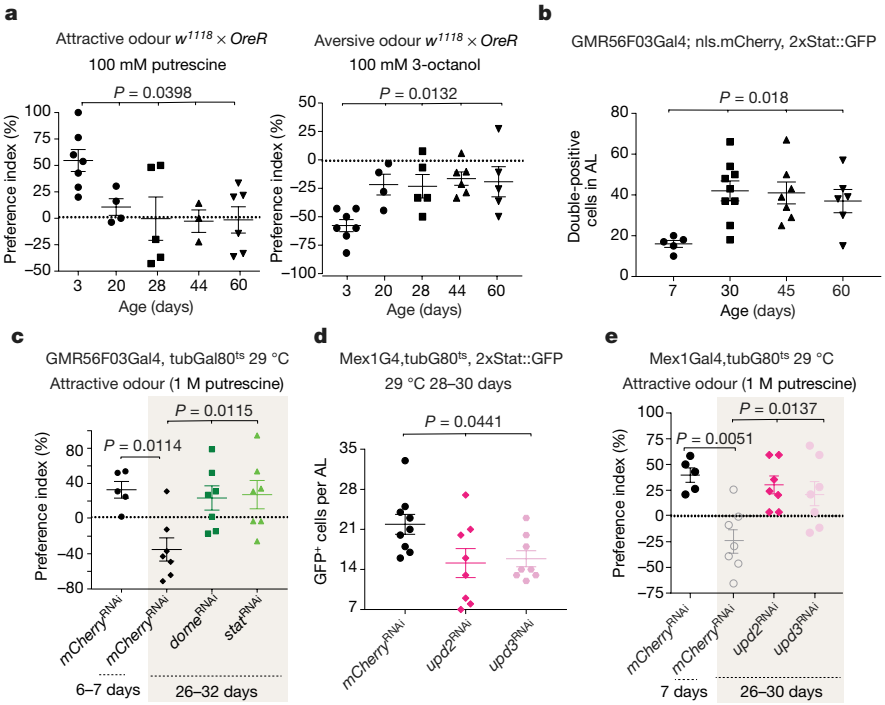

Fig. 2 | Chronic activation of JAK–STAT signalling in old EGs causes decline of olfaction sensitivity during ageing. a, Preference index of young and old wild-type (w^{1118} × *OreR*) flies. **b**, 2xSTAT::GFP expression in the EG at the AL during ageing. Images are shown in Extended Data Fig. 5c. **c**, Preference index of young control flies and of old flies with indicated perturbations in the EG. **d**, Numbers of 2xSTAT::GFP$^+$ glia per AL of old flies with indicated perturbation in enterocytes. Images are shown in Extended Data Fig. 5f. **e**, Preference index of young control flies and of old flies with indicated perturbations in enterocytes. Data are mean and s.e.m. n = 7, 4, 5, 3 and 6 independently performed experiments per condition (from left to right) in **a**, n = 5, 9, 7 and 6 brains per condition (from left to right) in **b**, n = 5, 7, 7 and 7 independently performed experiments per condition (from left to right) in **c**, n = 9, 8 and 8 brains per condition (from left to right) in **d**, n = 5, 7, 7 and 7 independently performed experiments per condition (from left to right) in **e**. Data in **b** and **d** are representative of two independently performed experiments. P values from two-tailed Mann–Whitney test in **c** and **e** when comparing young and old *mCherry*^{RNAi}; other P values from Kruskal–Wallis test.

using UAS::mCD4GFP) of EG at the AL (Extended Data Fig. 2f), and glomerular compartmentalization in the AL and lobe size remained unaffected (Extended Data Fig. 2f). JAK–STAT activation in EG was sufficient and required for infection-induced changes in olfactory discrimination, as overexpression of constitutively active Hop (*hop*^{tuml}) in EG reduced olfactory discrimination (Fig. 1e), whereas loss of Dome or STAT in all glia (repo::Gal4), or specifically in EG (GMR56F03::Gal4), rescued the decline of olfactory discrimination caused by *Ecc15* infection (Fig. 1e, Extended Data Fig. 3a, b). Overexpression of *hop*^{tuml} in EG also reduced ingestion of *Ecc15*-containing food and promoted survival of flies fed *PE*-containing food, whereas knockdown of Dome or STAT in EG increased ingestion of *Ecc15*-containing food in infected flies and increased mortality on *PE*-containing food (Fig. 1f, Extended Data Fig. 3d–h). We propose that the corresponding changes in ingestion of *PE*-laced food contribute to reduced mortality, but it is possible that additional genetic background conditions influence mortality, as seen, for example, in *Orco*-mutant flies, which ingest less bacteria (Extended Data Fig. 1g) but show increased susceptibility to *PE* (Extended Data Fig. 3i).

Gut-derived Upd proteins regulate olfaction

To test whether gut-derived Upd proteins directly contribute to the infection-induced activation of JAK–STAT signalling in EGs, we used intestinal enterocyte-specific perturbations using Mex1::Gal4, an enterocyte driver with no expression in the brain (Extended Data Fig. 4a, b). Indeed, JAK–STAT activation in glia at the AL could be triggered in naive flies or prevented in infected flies by overexpression or knockdown, respectively, of Upd2 and Upd3 in enterocytes (Fig. 1g, Extended Data Fig. 4c, d). Consistently, enterocyte-derived Upd2 and Upd3 were sufficient and required for the modulation of olfactory discrimination caused by infection (Fig. 1h, Extended Data Fig. 4e–g). Knockdown of Upd2 or Upd3 did not affect olfaction in naive flies (Extended Data Fig. 4f), and perturbing these ligands in fatbody (cg::Gal4) or haemocytes (hml::Gal4)—tissues that are sources for Upd proteins in other contexts[18,19]—did not significantly affect STAT activity in glia at the AL (Extended Data Fig. 4h–k).

Chronic JAK activation impairs ageing EG

Loss of olfactory sensitivity is an early sign of normal ageing and neurodegeneration[20]. In ageing *Drosophila*, olfactory perception has been reported to deteriorate before vision[11], a decline that we were able to recapitulate in our T-maze assays (Fig. 2a). Glomerular compartments in the AL became less organized and less distinct in geriatric (60–70-day-old) flies (Extended Data Fig. 5a) and AL size increased with age (Extended Data Fig. 5b). This correlates with a reduction in the number of EG and of glial membranous processes (Extended Data Fig. 5b), changes that are expected to affect AL structure[10], and thus probably contribute to the age-related decline in olfaction.

Ageing in *Drosophila* is accompanied by the development of intestinal inflammation, and is associated with the constitutive expression and release of Upd cytokines[21]. Consistently, JAK–STAT activity in the AL of EG was increased in old flies (Fig. 2b, Extended Data Fig. 5c), and knockdown of Dome or STAT by RNA interference (RNAi) in EG specifically (Fig. 2c, Extended Data Fig. 5d) or in all glia (Extended Data Fig. 5d) rescued the decline of olfactory discrimination in old flies. The loss of Dome in EG also rescued the age-related decline of EGs and restored

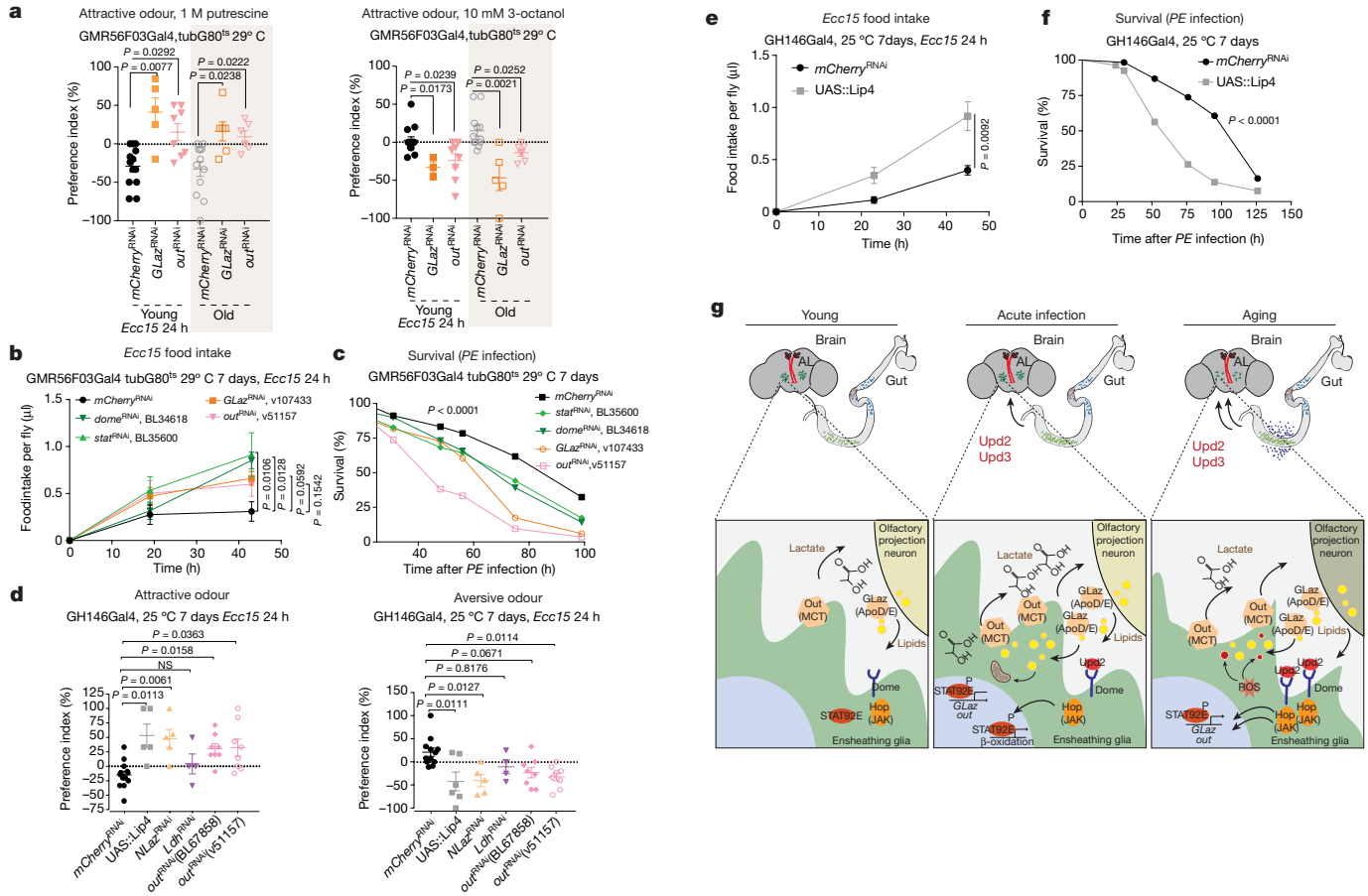

Fig. 3 | Disrupting the glia and neuron lactate shuttle in the AL aggravates infection-caused mortality, yet partially alleviates age-related olfactory degeneration. a, Preference index of young infected flies and of old flies after knockdown of the indicated genes in the EG. **b**, *Ecc15*$^{+}$ food intake of young infected flies after knockdown of the indicated genes in the EG. **c**, Survival curve of young flies upon continuous *PE* infection after knockdown of the indicated genes in the EG. **d**, Preference index of young infected flies with indicated perturbation in projection neurons. **e**, *Ecc15*$^{+}$ food intake of young infected flies overexpressing Lip-4 in projection neurons. **f**, Survival curve of flies overexpressing Lip-4 after continuous *PE* infection. Data are mean and s.e.m. $n = 13, 5, 8, 12, 6$ and 6 independently performed experiments per condition (from left to right) in **a** (left), $n = 14, 3, 8, 12, 5$ and 6 independently performed experiments per condition (from left to right) in **a** (right), $n = 8, 8, 8, 7$ and 6 replicates (3 flies per cohort) per condition for *mCherry*^{RNAi}, *dome*^{RNAi}, *stat*^{RNAi}, *GLaz*^{RNAi} and *out*^{RNAi}, respectively in **b**, $n = 102, 120, 104, 132$ and 84 flies for *mCherry*^{RNAi}, *dome*^{RNAi}, *stat*^{RNAi}, *GLaz*^{RNAi} and *out*^{RNAi} respectively in **c**, $n = 13, 5, 5, 4, 8$ and 8 independently performed experiments per condition (from left to right) in **d** (left), $n = 13, 6, 5, 4, 8$ and 8 independently performed experiments per condition (from left to right) in **d** (right), $n = 8$ replicates (3 flies per cohort) per condition in **e**, $n = 61$ and 80 flies for *mCherry*^{RNAi} and Lip-4 correspondingly in **f**. Data in **b** and **c** are representative of two independently performed experiments, and those shown in **e** and **f** are representative from three separate experiments. *P* values from two-tailed Mann–Whitney test in **e**; *P* values in **c** and **f** from log-rank test; other *P* values from Dunn's multiple comparisons test. NS, not significant ($P > 0.9999$ in **d**). **g**, Model for the effect of gut-derived cytokines on metabolic coupling of neurons and glia at the AL.

the size of the AL (Extended Data Fig. 5e). JAK–STAT activation in the EG of old flies is a consequence of intestinal Upd release, as knocking down Upd2 and Upd3 in enterocytes alleviated STAT activation in the AL (Fig. 2d, Extended Data Fig. 5f), and prevented the age-related decline of olfactory discrimination (Fig. 2e, Extended Data Fig. 5g).

This age-related decline of olfactory discrimination was independent of the microbiota, as germ-free old flies still exhibited reduced olfaction sensitivity, increased JAK–STAT signalling in the AL, decreased numbers of EG, loss of glial cellular processes, and an enlarged AL (Extended Data Fig. 6a–d). These results are consistent with the observation that the age-related increase in Upd released from the gut is also independent of the microbiota[21].

To understand why EG but not other glia selectively respond to Upd ligands and activate JAK–STAT signalling during ageing or infection, we performed single-cell RNA sequencing (scRNA-seq) on purified glia from young and old flies. Either all glia (labelled using repo::Gal4) or EG selectively (labelled using GMR56F03::Gal4) were profiled using Smart-seq2 (Extended Data Fig. 7a, b). The expression of *dome* was significantly higher in EG than in other glia (Extended Data Fig. 7c), consistent with the specific upregulation of *socs36E*, a known target of JAK–STAT signalling, in EG but not in other glia during ageing (Extended Data Fig. 7d). These results are supported by a similar upregulation of *Socs36E* in EG of old flies observed in a previous scRNA-seq dataset[22] (Extended Data Fig. 7e, f).

Glial JAK reprograms lipid metabolism

Bulk RNA sequencing analysis on glia (repo::Gal4, UAS::tdTomato) purified from central brains of flies expressing a 10xSTAT::GFP reporter[16] (Extended Data Fig. 7g, Supplementary Fig. 1) revealed that the transcriptomes of STAT::GFP^{+} glia from *Ecc15* infected and uninfected flies were more similar to each other than to STAT::GFP^{-} glia of either condition, which indicates that JAK–STAT induction has a stronger influence on glial transcriptomes than other infection-related changes (Extended Data Fig. 7h). Differentially expressed genes (866 genes using a cut-off of two-fold change, $P < 0.001$, false discovery rate (FDR) < 0.01 and reads > 0.5)

(Extended Data Fig. 7i, Supplementary Table 2) were significantly enriched in genes that encode proteins involved in lipid metabolism and carbohydrate transmembrane transport (Extended Data Fig. 7j). These included the lipid binding protein glial lazarillo (GLaz, a homologue of apolipoprotein D in mammals[23]), which facilitates lipid transport from neurons to glia in flies[23], the lipid droplet surface binding proteins Lsd-1 and Lsd-2[24,25], the diacylglycerol O-acyltransferase Midway, which is a central regulator of triacylglycerol biosynthesis[26], and Coatomer, which is responsible for protein delivery to lipid droplets (LDs)[27] (Extended Data Fig. 7k). This induction of lipid storage genes was coupled with induction of the monocarboxylate transporter (MCT) Outsiders (Out), and the MCT accessory protein Basigin (Bsg), sugar transporters (Tret1-1 and Tret1-2), and 17 enzymes involved in β-oxidation (Extended Data Fig. 7l–n).

Glial MCTs promote lipid production in neurons and LD accumulation in glia by establishing a neuron and glia 'lactate shuttle'[23]. To test a potential role for STAT signalling in influencing this shuttle at the AL, we assessed the accumulation of LDs at the AL in infected young flies using a combination of a neutral lipid probe (LipidTox, deep red) and a lipid peroxidation probe (C11-Bodipy, 581/591). We observed a transient accumulation of LDs 24 h after infection, which decreased 4 days after infection (Extended Data Fig. 8a), possibly owing to increased levels of β-oxidation[28] (Extended Data Fig. 7m, n). Overexpression of *hop*^{tuml} in the EG of young flies also promoted LD accumulation (Extended Data Fig. 8b), whereas knocking down Dome or STAT rescued infection-induced accumulation (Extended Data Fig. 8c). GLaz and Out were required for LD accumulation after infection (Extended Data Fig. 8c), and overexpression of Upd2 and Upd3 in the gut induced LD accumulation at the AL, whereas knockdown of Upd2 or Upd3 alleviated LD accumulation in infected flies (Extended Data Fig. 8d; efficiency of RNAi knockdown was confirmed by qPCR, Extended Data Fig. 8e, f). Infection or JAK–STAT perturbation did not influence lipid peroxidation in LDs in young flies (Extended Data Fig. 8g, h).

Lipotoxicity due to chronic JAK activity

During neuronal stress, neurons can preferentially transfer fatty acids to glia, causing lipid accumulation and increasing fatty acid β-oxidation in glia[28,29]. We observed a significant induction of LDs specifically in EG at the AL in old flies (Extended Data Fig. 9a), phenocopying *hop*^{tuml} overexpression (Extended Data Fig. 8b). As fatty acid β-oxidation is a source of reactive oxygen species (ROS)[28,30] that can result in lipid peroxidation, and lipid peroxidation in pigment cells (glia of the retina) promotes the demise of photoreceptors in the retina[29], whereas oxidative stress contributes to age-related dysfunction of cholinergic projection neurons within the olfactory circuit[11], we reasoned that overall levels of ROS might increase in glia with age. We expressed various genetically encoded ROS sensors in all glia (repo::Gal4) or in EG only (GMR56F03::Gal4) to measure levels of hydrogen peroxide (H_2O_2; measured by RoGFP2_Orp1) or the glutathione redox potential (measured by RoGFP2_Grx1) within the mitochondria or cytosol, respectively. Cytosolic levels of H_2O_2 were increased in the EG of old flies (both cytosolic and mitochondrial H_2O_2 levels were increased in all glia), whereas the cytosolic glutathione redox potential remained unchanged (Extended Data Fig. 9b–e). In contrast to acute intestinal infection in young flies, lipids were peroxidated in LDs of old flies (Extended Data Fig. 9f). Knocking down STAT specifically in EG, or knocking down Upd2 and Upd3 in gut enterocytes, inhibited LD accumulation and alleviated lipid peroxidation in old flies (Extended Data Fig. 9f, g).

Olfactory discrimination was partially rescued in old and young infected flies after knockdown of GLaz and Out in EG (Fig. 3a, Extended Data Fig. 10a). Knockdown of GLaz and Out also led to more *Ecc15* food consumption, increased mortality after *PE* exposure, and reduced LD accumulation in the glia of old flies (Fig. 3b, c, Extended Data Fig. 10b–e).

To confirm that infection or ageing-induced metabolic changes in EG affect neuron or glia metabolic coupling at the AL, we assessed the consequences of perturbing projection neurons directly using GH146::Gal4. Knocking down Out but not lactate dehydrogenase (Ldh) in projection neurons rescued olfactory discrimination of infected or aged flies (Fig. 3d, Extended Data Fig. 10f), whereas food preference or mortality was not influenced (Extended Data Fig. 10g, h). Overexpression of lipase 4 (Lip-4) in projection neurons, or knockdown of the neuronal lipid binding protein neural lazarillo (NLaz), significantly improved olfactory discrimination in infected or old flies (Fig. 3d, Extended Data Fig. 10f), and overexpression of Lip-4 increased *Ecc15* food consumption and increased mortality after PE exposure (Fig. 3e, f, Extended Data Fig. 10i).

Discussion

Our work suggest that gut-derived inflammatory cytokines modulate the metabolic coupling of glia and neurons in the brain of *Drosophila* to induce an adaptive temporary halt of olfactory discrimination after intestinal infection, but also contribute to age-related olfactory decline (Fig. 3g). We propose that gut-derived Upd2 and Upd3 reprogram lipid metabolism in EG, increasing lactate and lipid transport between glia and olfactory neurons, resulting in LD accumulation and upregulation of mitochondrial β-oxidation, potentially a source of increased ROS production. Chronic activation of this metabolic shift in old flies results in the accumulation of peroxidated lipids in EG, promoting their decay and contributing to the previously described functional decline of olfactory neurons[11]. Detailed characterization of this metabolic reprogramming, and further exploration of the role of lipid synthesis in projection neurons for glial lipid accumulation and for olfactory discrimination are important avenues for further study.

Our findings further determine the regulation of avoidance behaviour against enteropathogens in insects. In addition to gustatory bitter neurons[5] and immune receptors in octopaminergic neurons[3], Upd proteins constitute a direct endocrine signal from the damaged intestinal epithelium in this complex but essential behaviour. We propose that Upd-mediated suppression of olfactory discrimination is required to prevent olfaction-mediated attraction to a food source after pathogenicity has been established and aversion is induced by gustatory neurons[5]. It remains unclear, however, whether gustatory neurons are also affected by JAK–STAT signalling in EG. Whether similar mechanisms are conserved and control infection-induced loss of sensory perception in vertebrates including humans[1,31,32] will be interesting to explore.

Online content

Any methods, additional references, Nature Research reporting summaries, source data, extended data, supplementary information, acknowledgements, peer review information; details of author contributions and competing interests; and statements of data and code availability are available at https://doi.org/10.1038/s41586-021-03756-0.

1. Wang, A. et al. Opposing effects of fasting metabolism on tissue tolerance in bacterial and viral inflammation. *Cell* **166**, 1512–1525 (2016).
2. Ayres, J. S. & Schneider, D. S. The role of anorexia in resistance and tolerance to infections in *Drosophila*. *PLoS Biol*. **7**, e1000150 (2009).
3. Kobler, J. M., Rodriguez Jimenez, F. J., Petcu, I. & Grunwald Kadow, I. C. Immune receptor signaling and the mushroom body mediate post-ingestion pathogen avoidance. *Curr. Biol*. **30**, 4693–4709.e3 (2020).
4. Stensmyr, M. C. et al. A conserved dedicated olfactory circuit for detecting harmful microbes in *Drosophila*. *Cell* **151**, 1345–1357 (2012).
5. Charroux, B., Daian, F. & Royet, J. *Drosophila* aversive behavior toward erwinia carotovora carotovora is mediated by bitter neurons and leukokinin. *iScience* **23**, 101152 (2020).
6. Soria-Gomez, E., Bellocchio, L. & Marsicano, G. New insights on food intake control by olfactory processes: the emerging role of the endocannabinoid system. *Mol. Cell. Endocrinol*. **397**, 59–66 (2014).
7. Soria-Gómez, E. et al. The endocannabinoid system controls food intake via olfactory processes. *Nat. Neurosci*. **17**, 407–415 (2014).
8. Liang, L. & Luo, L. The olfactory circuit of the fruit fly *Drosophila melanogaster*. *Sci. China Life Sci*. **53**, 472–484 (2010).

9. Liu, H. et al. Astrocyte-like glial cells physiologically regulate olfactory processing through the modification of ORN-PN synaptic strength in *Drosophila*. *Eur. J. Neurosci.* **40**, 2744–2754 (2014).
10. Wu, B., Li, J., Chou, Y. H., Luginbuhl, D. & Luo, L. Fibroblast growth factor signaling instructs ensheathing glia wrapping of *Drosophila* olfactory glomeruli. *Proc. Natl Acad. Sci. USA* **114**, 7505–7512 (2017).
11. Hussain, A. et al. Inhibition of oxidative stress in cholinergic projection neurons fully rescues aging-associated olfactory circuit degeneration in *Drosophila*. *eLife* **7**, e32018 (2018).
12. Wu, S. C., Cao, Z. S., Chang, K. M. & Juang, J. L. Intestinal microbial dysbiosis aggravates the progression of Alzheimer's disease in *Drosophila*. *Nat. Commun.* **8**, 24 (2017).
13. Keshavarzian, A., Engen, P., Bonvegna, S. & Cilia, R. The gut microbiome in Parkinson's disease: a culprit or a bystander? *Prog. Brain Res.* **252**, 357–450 (2020).
14. Jiang, H. et al. Cytokine/Jak/Stat signaling mediates regeneration and homeostasis in the *Drosophila* midgut. *Cell* **137**, 1343–1355 (2009).
15. Tracy Cai, X. et al. AWD regulates timed activation of BMP signaling in intestinal stem cells to maintain tissue homeostasis. *Nat. Commun.* **10**, 2988 (2019).
16. Bach, E. A. et al. GFP reporters detect the activation of the *Drosophila* JAK/STAT pathway in vivo. *Gene Expr. Patterns* **7**, 323–331 (2007).
17. Freeman, M. R. *Drosophila* central nervous system glia. *Cold Spring Harb. Perspect. Biol.* **7**, a020552 (2015).
18. Chakrabarti, S. et al. Remote control of intestinal stem cell activity by haemocytes in *Drosophila*. *PLoS Genet.* **12**, e1006089 (2016).
19. Rajan, A. & Perrimon, N. *Drosophila* cytokine unpaired 2 regulates physiological homeostasis by remotely controlling insulin secretion. *Cell* **151**, 123–137 (2012).
20. Doty, R. L. & Kamath, V. The influences of age on olfaction: a review. *Front. Psychol.* **5**, 20 (2014).
21. Li, H., Qi, Y. & Jasper, H. Preventing age-related decline of gut compartmentalization limits microbiota dysbiosis and extends lifespan. *Cell Host Microbe* **19**, 240–253 (2016).
22. Davie, K. et al. A single-cell transcriptome atlas of the aging *Drosophila* brain. *Cell* **174**, 982–998.e20 (2018).
23. Liu, L., MacKenzie, K. R., Putluri, N., Maletić-Savatić, M. & Bellen, H. J. The glia-neuron lactate shuttle and elevated ROS promote lipid synthesis in neurons and lipid droplet accumulation in glia via APOE/D. *Cell Metab.* **26**, 719–737.e6 (2017).
24. Fauny, J. D., Silber, J. & Zider, A. *Drosophila* Lipid Storage Droplet 2 gene (*Lsd-2*) is expressed and controls lipid storage in wing imaginal discs. *Dev. Dyn.* **232**, 725–732 (2005).
25. Men, T. T., Binh, T. D., Yamaguchi, M., Huy, N. T. & Kamei, K. Function of Lipid storage droplet 1 (Lsd1) in wing development of *Drosophila melanogaster*. *Int. J. Mol. Sci.* **17**, E648 (2016).
26. Kühnlein, R. P. Thematic review series: Lipid droplet synthesis and metabolism: from yeast to man. Lipid droplet-based storage fat metabolism in *Drosophila*. *J. Lipid Res.* **53**, 1430–1436 (2012).
27. Soni, K. G. et al. Coatomer-dependent protein delivery to lipid droplets. *J. Cell Sci.* **122**, 1834–1841 (2009).
28. Ioannou, M. S. et al. Neuron-astrocyte metabolic coupling protects against activity-induced fatty acid toxicity. *Cell* **177**, 1522–1535 (2019).
29. Liu, L. et al. Glial lipid droplets and ROS induced by mitochondrial defects promote neurodegeneration. *Cell* **160**, 177–190 (2015).
30. Rosca, M. G. et al. Oxidation of fatty acids is the source of increased mitochondrial reactive oxygen species production in kidney cortical tubules in early diabetes. *Diabetes* **61**, 2074–2083 (2012).
31. Brann, D. H. et al. Non-neuronal expression of SARS-CoV-2 entry genes in the olfactory system suggests mechanisms underlying COVID-19-associated anosmia. *Sci. Adv.* **6**, eabc5801 (2020).
32. Salmon Ceron, D. et al. Self-reported loss of smell without nasal obstruction to identify COVID-19. The multicenter Coranosmia cohort study. *J. Infect.* **81**, 614–620 (2020).

Publisher's note Springer Nature remains neutral with regard to jurisdictional claims in published maps and institutional affiliations.

© The Author(s), under exclusive licence to Springer Nature Limited 2021

Methods

Drosophila stocks and husbandry

Flies were kept on standard fly food which were prepared with the following recipe: 1 l distilled water, 22 g molasses, 6.26 ml propionic acid, 13.8 g agar, 80 g corn flour, 75 g malt extract, 18 g inactivated dry yeast, 10 g soy flour, 2 g methyl 4-hydroxybenzoate in 7.2 ml of ethanol. Flies were reared at the temperature indicated in corresponding figures and at 65% humidity with a 12 h light/dark cycle, except for sterile flies and conventional control flies, which were reared at room temperature with no tight control on humidity and light/dark cycle. Only female flies were used in all experiments.

The Gal4-UAS target expression system was used to conditionally express UAS-linked transgenes in the presence of indicated Gal4. Crosses with tub::G80^{ts} were maintained at 18 °C on standard fly food and 3-day-old female adults were transferred to 29 °C to temporarily induce transgene expression, unless otherwise indicated. Crosses without tub::G80^{ts} were maintained at 25 °C on standard fly food.

This study follows all ethical regulations required for research using *Drosophila melanogaster* as an experimental model. Complying with NIH regulations, no ethical approval was required for work with *D. melanogaster*.

The following fly lines were obtained from Bloomington *Drosophila* Stock Center: *w*^{1118}, *Oregon-R* (*OreR*), *Gr63a*^{1} (9941), *Orco*^{1} (23129), *mCherry*^{RNAi} (35785), UAS::*hop*^{tuml}/FM7c (8492), *upd2*^{RNAi} (33988), *upd2*^{RNAi} (33949), *dome*^{RNAi} (34618), *stat*^{RNAi} (35600), *ldh*^{RNAi} (33640), GMR54H02Gal4 (45784), GMR54C07Gal4 (50472), GMR86E01Gal4 (45914), GMR56F03Gal4 (39157), UAS::LacZ (1776), UAS::nls.mCherry (38425), GMR10E12Gal4 (46517), SPARCGal4 (77473), GMR83E12Gal4 (40363), TubG80^{ts} (7013), 10xSTAT::GFP (26198), repoGal4 (7415), UAS::lipase-4 (67142), GH146Gal4 (30026), *out*^{RNAi} (67858), UAS::MitoRoGFP2_Orp1 (67667), nSybGal4 (51635), UAS::mCD8-GFP (5137), actin::Gal4 (4414), hmlGal4, UAS::2xGFP (30140), UAS::2xGFP (60292).

The following fly lines were obtained from Vienna *Drosophila* RNAi Center: *dome*^{RNAi} (106071), *stat*^{RNAi} (106980), *GLaz*^{RNAi} (15387), *GLaz*^{RNAi} (107433), *upd3*^{RNAi} (27134), *NLaz*^{RNAi} (35558) and *out*^{RNAi} (51157).

The following fly lines were gifts from other laboratories: 2xSTAT::GFP (E. Bach), *LacZ*^{RNAi} (M. Miura), UAS:: *hop*^{tuml}/cyo (D. Bilder), *upd3*^{RNAi} (S. Hou), UAS::upd2 (M. Zeidler), UAS::upd3 (N. Buchon), UAS::CD4GFP,UAS::RedStinger/Tm6 (L. Luo), NP1Gal4 (D. Ferrandon), Mex1Gal4;tubG80^{ts} (L. O'Brien), UAS::tdTomato (M. A. Welte), cg::Gal4 (C. S. Thummel), UAS::CytoRoGFP2_Orp1 and UAS::CytoRoGFP2_Grx1 (T. Dick).

The genotypes, ages and genders of flies used in each figure are detailed in Supplementary Table 1. Knockdown efficiencies of the RNAi lines used in this paper are shown in Extended Data Figs. 3c, 4g, 8e, f.

Starvation and bacterial infection

Bacterial strains, *Ecc15* or *PE*, were cultured in LB medium at 29 °C for 18–24 h. Bacteria were centrifuged at 4,600*g*, room temperature for 10 min and resuspended in 500 µl 5% sucrose (OD_{100}). Bacteria sucrose solution was then added to empty fly vials containing Whatman filter paper at the bottom. Flies were starved in empty vials for 2–3 h before transferred to vials containing bacteria solution, except for overnight wet starvation, during which flies were starved in vials containing 500 µl ddH_2O on Whatman filter paper. Flies were infected with *Ecc15* for 4 h or 24 h as noted correspondingly, before the dissection or use in assays. To infect flies with heat-killed *Ecc15*, *Ecc15* sucrose solution was boiled at 95 °C for 30 min, and cooled down before use. Mock flies were treated identically, but fed with 500 µl 5% sucrose without bacteria only. For *PE* survival experiments, flies were infected in vials containing 500 µl *PE* sucrose solution on Whatman filter paper continuously, and 100 µl 5% sucrose was added every day to vials until the end point.

Axenic fly culture

Sterile flies were generated and aged under sterile conditions as previously described[21]. In brief, embryos collected on sterile apple juice agar plates (recipe: 700 ml H_2O, 22.5 g agar, 250 ml apple juice, 25 g sucrose, 7 ml 20% methyl 4-hydroxybenzoate in ethanol) were bleached for 3 min in 2.7% sodium hypochlorite (twofold diluted bleach), and washed twice with sterile ddH_2O for 1 min. To make conventional control flies, collected eggs were washed with same amount of ddH_2O instead as above. These embryos were transferred into sterile food in a tissue culture hood, followed by adding 100 µl of sterile 70% glycerol on top. Flies were maintained in a laminar flow hood and flipped into new sterile food every 2–3 days. To validate axenic conditions, adult fly guts were dissected and plated onto nutrient agar plates to check commensal loads.

Immunostaining

Adult female *Drosophila* heads were dissected in 1× pH 7.4 PBS, and fixed for 20 min at room temperature in fixation buffer containing: 1× PBS and 4% formaldehyde. Heads were washed in washing buffer (1× PBS, 0.1% Triton X-100) for 1 h (20 min each, 3 times), followed by incubation in blocking buffer (1× PBS, 0.1% Triton X-100, 5% donkey serum) at room temperature for 1 h. Samples were incubated in primary antibodies for two nights at 4 °C, followed by 1.5-h washing at room temperature (30 min each, three times), and secondary antibody incubation for 2 h at room temperature.

Adult female *Drosophila* guts were dissected in 1× pH 7.4 PBS, and fixed for 20–30 min at room temperature in fixation buffer containing: 25 mM KCl, 100 mM glutamic acid, 1 mM $MgCl_2$, 20 mM $MgSO_4$, 4 mM sodium phosphate, and 4% formaldehyde. Guts were washed for 1 h at 4 °C in washing buffer containing: 1× PBS, 0.5% bovine serum albumin and 0.1% Triton X-100, followed by incubation in primary antibodies overnight at 4 °C, 1 h washing at 4 °C, and secondary antibodies for 2 h at room temperature.

For neutral lipid droplet staining, brains were dissected and fixed as above, followed by 30 min wash in washing buffer. Brains were stained with HCS LipidTOX Deep Red neutral lipid stain (ThermoFisher, H34477, 1:200 diluted in 1× PBS) on an orbital shake at room temperature overnight. Following one wash with 1× PBS, brains were mounted with SlowFade Gold Antifade Mountant (ThermoFisher, S36936) and imaged on the same day.

Primary antibodies and dilution used in this study: mouse anti-repo (DSHB 8D12, 1:100) labelling glia in the central brain[33], mouse anti-NC82 (DSHB, 1:50–1:100), rabbit anti-GFP (ClonTech, 632592, 1:500). Fluorescent secondary antibodies were bought from Jackson Immunoresearch. DAPI was used to stain DNA at 1:1,000. All the images were taken on the Yokogawa CSU-W1/Zeiss 3i Marianas spinning disk confocal microscope with Hamamatsu FLASH 4.0 sCMOS camera, under 40× objective, except for live imaging (described below). All the images were processed by Adobe Illustrator 2020 and Image J.

Ex vivo live imaging of *Drosophila* brains

Adult female flies were dissected in adult haemolymph-like saline (AHLS) culture medium containing 2 mM $CaCl_2$, 5 mM KCl, 5 mM HEPES, 8.2 mM $MgCl_2$, 108 mM NaCl, 4 mM $NaHCO_3$, 1 mM NaH_2PO_4, 5 mM trehalose and 10 mM sucrose. Brains were transferred to a 35-mm glass bottom dish (MatTek, P35G-1.5-14-C), with 50–100 µl 3% low melting agarose (dissolved in AHLS medium) added on top. After 5 min, 3 ml AHLS medium was added in the dish, and brains were imaged on the Yokogawa CSU-W1/Zeiss 3i Marianas spinning disk confocal microscope with Photometrics Evolve EMCCD camera under 40× objective. For ratiometric CytoRoGFP2_Orp1, MitoRoGFP2_Orp1 and CytoRoGFP2_Grx1 biosensors[34], probe fluorescence was excited sequentially using the 405-nm and 488-nm laser lines and emission was detected at 500–550 nm. Imaging settings were carefully optimized before each experiment

to ensure optimal dynamic range without saturating cameras. Identical *z*-stacks were acquired for each sample.

For lipid peroxidation staining and imaging, fly brains were dissected in Shields and Sang M3 insect medium (Sigma, S8398) and incubated for 30 min in this medium containing LipidTox Deep Red (1:200) and 2 μM C11- BODIPY 581/591 (Invitrogen, D3861) at 37 °C. Following two rinses with 1× PBS, brains were mounted with SlowFade Gold Antifade Mountant and imaged immediately with Yokogawa CSU-W1/Zeiss 3i Marianas spinning disk confocal microscope possessing Photometrics Evolve EMCCD camera, under 40× objective. Identical *z*-stacks were acquired for each sample. Lipid peroxidation were determined by the intensity of oxidized lipids (excitation: 488 nm, emission: 500–540 nm) over the intensity of non-oxidized lipids (excitation: 561 nm, emission: 570–610 nm).

Glia sorting, bulk RNA sequencing and data analysis

Approximately 100 brains were dissected for each replicate in cold Shields and Sang M3 insect medium (Sigma, S8398) containing 10% fetal bovine serum (FBS; ThermoFisher, 16000036). Brains were dissociated in the solution containing 300 μl papain (Sigma, P4762; dissolved in 1× PBS to a final concentration of 100 U ml^{-1}) and 4.1 μl liberase TM solution (Roche, 5401119001; reconstituted with 1× PBS to a final centration of 2.5 mg ml^{-1}) at 25 °C, 1,000 rpm for 20 min, as previously described[35]. Cells were stained with Calcein blue (ThermoFisher, c1429, 1:1,000) for 20 min on ice, washed, and resuspended in dissection buffer with SYTOX Deep Red Dead cell stain (ThermoFisher, S11381, 1:1,000). GFP^+ $tdTomato^+$ cells and GFP^- $tdTomato^+$ cells were sorted into Trizol (ThermoFisher, 15596026) respectively, using fluorescence activated cell sorting (FACS) with BD FACSAria Fusion (gating strategy is shown in Supplementary Fig. 1), followed by RNA extraction. cDNA was generated from 2 ng of RNA using Smart-Seq V4 Ultra Low Input RNA Kit (Takara, 634894). Then, 150 pg of cDNA was used to make sequencing libraries by Nextera XT DNA Sample Preparation Kit (Illumina, FC-131-1024). Libraries were sequenced for 50 single read cycles and 30 million reads per sample on Illumina NovaSeq 6000. Reads were aligned to *Drosophila* genome (version BDGP6), using the GSNAP aligner as part of the HTSeqGenie R package (version 4.2). Reads that uniquely aligned within exonic boundaries of genes were used to derive expression estimates. nRPKM values, in which total library sizes were normalized using the median ratio method as previously described[36], were generated for each gene. Differential gene expression analysis was performed in Partek Flow (Partek) and Gene Ontology analysis was done using tools at Flymine.org and Geneontology.org. A list of differentially expressed genes shown in Extended Data Fig. 7i is shown in Supplementary Table 2.

scRNA-seq using Smart-seq2 and data analysis

Approximately 80–100 adult female flies at 5 or 50 days old that overexpressed mCD8::GFP specifically in glia (using repo::Gal4) or in EG (using GMR56F03::Gal4) were dissected, respectively, in cold Shields and Sang M3 insect medium (Sigma S8398) containing 10% FBS (ThermoFisher, 16000036). To improve glial dissociation efficiency and viability for Smart-seq2, we compared different enzyme combinations, including papain, liberase, collagenase and trypsin, and found that the combination of collagenase and trypsin performed the best. To make 1 ml dissociation buffer, we mixed 250 μl collagenase (2.5 mg ml^{-1}; Sigma, C9891), 100 μl trypsin EDTA (0.05%), and 650 μl 1× PBS. Brains were dissociated at 25 °C, 1,000 rpm for 30 min (samples were pipetted 50–100 times every 10 min). After single-cell suspensions were prepared, GFP^+ cells were FACS sorted into individual wells of 384-well plates using SH800 (Sony Biotechnology). Full-length poly(A)-tailed RNA was reverse-transcribed and amplified by PCR following the Smart-seq2 protocol[37]. cDNA was digested using lambda exonuclease (New England Biolabs) and then amplified for 25 cycles. Sequencing libraries were prepared from amplified cDNA, pooled, and quantified using BioAnalyser (Agilent). Sequencing was performed using the Novaseq 6000 Sequencing system (Illumina) with 100 paired-end reads and 2 × 8-bp index reads.

Reads were aligned to the *Drosophila* genome (r6.10) using STAR (2.5.4)[38]. Gene counts were produced using HTseq (0.11.2) with default settings except '-m intersection-strict'[39]. We removed low-quality cells having fewer than 10,000 uniquely mapped reads. To normalize for differences in sequencing depth across individual cells, we rescaled gene counts to counts per million reads (CPM). All analyses were performed after converting gene counts to logarithmic space via the transformation $\log_2(CPM + 1)$. For data visualization, we performed principal component analysis (PCA) on the cell × gene matrix and used *t*-distributed stochastic neighbour embedding (*t*-SNE) to further project the top 50 principal components into a two-dimensional space. Figures were generated using scanpy in Python (v.2.7).

For data analysis in Extended Data Fig. 7b, we manually curated the non-ensheathing glial (non-EG) population. Repo::Gal4 labels all glia, and some repo::$Gal4^+$ glial cells were clustered with EG clusters (GMR56F03::$Gal4^+$) as expected. These cells belong to $repo^+$ ensheathing glia. We validated these cells using EG markers. The repo::$Gal4^+$, GMR56F03::$Gal4^-$ cells were categorized as non-EG. Of note, a small number of GMR56F03::$Gal4^+$ cells appeared to be non-EG, presumably owing to the non-specificity of this Gal4 driver, which were excluded from the analysis. For analysis in Extended Data Fig. 7e, f, cells were extracted from a previously published dataset[22] in which 57,000 filtered brain cells that were sequenced using 10x Genomics platform.

Olfactory T-maze assay

For young flies with targeted gene overexpression or knockdown, experimental crosses were maintained at 18 °C, and 3–4-day-old progenies were transferred to 29 °C for another 5–7 days before T-maze assay. To age flies, wild-type flies (w^{1118} × *OreR*) were maintained at 25 °C. Experimental flies expressing $dome^{RNAi}$, $stat^{RNAi}$, $GLaz^{RNAi}$ or out^{RNAi} in the presence of GMR56F03Gal4;tubG80^{ts} were aged at 25 °C for 14–16 days followed by ageing at 29 °C for 10–14 days, unless otherwise specified. Experimental flies with $upd2^{RNAi}$ and $upd3^{RNAi}$ were aged at 29 °C during the adult life for 28–30 days, whereas flies expressing $NLaz^{RNAi}$, ldh^{RNAi}, out^{RNAi} and UAS::Lip-4 in projection neurons were aged at 25 °C for 36–40 days. Axenic flies were aged at room temperature in a tissue culture hood as described above. During each experiment, a cohort of 30–90 flies were tested per condition, the result of which was considered as one replicate and was indicated as one dot in the panel.

T-maze assay was performed in the dark at 22–24 °C and 35–40% humidity. Only female flies were tested, and flies were given 1 min to make a choice before counting. The attractive odour putrescine (Sigma, 51799), and the aversive odour 3-octanol (Sigma, 218405) were diluted by ddH_2O and paraffin oil (Sigma, 18512), respectively. Putrescine (100 mM) and 3-octanol (100 mM) were used for wild-type flies (w^{1118} × *OreR*), whereas putrescine (1 M) and 3-octanol (10 mM) were supplied to the rest of the genotypes. Odorant solution (50 μl) and control solution were sequentially added onto Whatman filter paper of the odorant tube and the control tube, before installed into the T-maze device. After experimentation, flies in the odorant tube and the control tube were counted. The preference index was calculated using the equation: preference index = $(N_{odour} - N_{control})/(N_{odour}) + N_{control}) \times 100\%$. Statistical analysis was performed using non-parametric Mann–Whitney test, Kruskal–Wallis test, or Dunn's multiple comparisons test in GraphPad Prism version 7.05.

CAFE assay

We modified the CAFE assay[40] by putting three flies in a transparent vial containing 1-cm high 1% agar at the bottom to keep the moisture. Two 5-μl capillaries were inserted into a cotton plug on top. One capillary contained liquid food, including 10% yeast, 10% sucrose and blue dye, and the other one contained liquid food mixed with *Ecc15*. To make

Ecc15-mixed liquid food, 40 ml *Ecc15* was freshly cultured as described above, and was resuspended in 3 ml liquid food. The food intakes were recorded at corresponding time points and the capillaries were changed every 24 h.

RT–qPCR

Twenty guts from Np1::Gal4 flies or ten heads from actin::Gal4 or nSyb::Gal4 flies were collected correspondingly in Trizol (Invitrogen) per biological replicate. cDNA was synthesized using iScript cDNA synthesis kit (Bio-Rad). Real-time qPCR was performed on a QuantStudio 8 Flex system (ThermoFisher) with the following Taqman Probes (ThermoFisher). For data analysis, C_t values of target genes in linear scale were normalized to actin5c.

Taqman probes: Dm01845230_g1 (*out*), Dm01821385_m1 (*GLaz*), Dm01844576_g1 (*NLaz*), Dm01841229_g1 (*Ldh*), Dm01844134_g1 (*upd2*), Dm01844142_g1 (*upd3*), Dm02361909_s1 (*actin5c*) were used.

Intracellular flow cytometry and FACs analysis

Twenty brains were dissected for each biological replicate. Single-cell suspension of each sample was prepared freshly, following the above dissociation step using the combination of papain and liberase. Cells was fixed, permeabilized and stained with anti-GFP antibody (ClonTech, 632592, 1:500) following a previously published protocol[15], using eBioscience Foxp3/Transcription Factor Staining Buffer Set (ThermoFisher, 00–5523–00). DAPI was added to each sample at a final concentration 1 μg ml^{-1}, to stain nuclei, and analysed by BD Symphony flow cytometer. Fluorescent secondary antibodies were bought from Jackson Immunoresearch (1:500).

FlowJo v.10 Software computed the median fluorescence intensity of GFP in $mCherry^+$ EG, and generated histogram (*x* axis: fluorescence intensity levels of channels of interest in logarithmic scale; *y* axis: the number of events, noted as modal). To overlay several cell populations with different sizes, the absolute cell counts were normalized to the peak height at mode of the distribution, noted as normalized to mode in *y* axis.

Image quantification and statistical analyses

Images taken on live brains with CytoRoGFP2_Orp1, MitoRoGFP2_Orp1 or MitoRoGFP2_Grx1 fluorescent biosensors were analysed with Image J. *z*-stack images were converted to maximal intensity projections. For ratiometric measurements of these biosensors, the 488 nm excitation channel was used for image segmentation and the detection of regions of interest (ROIs). For CytoRoGFP2_Orp1 and CytoRoGFP2_Grx1, ROIs were carefully selected to represent each single glia at the AL manually, and automated ROI detection was optimized and used for MitoRoGFP2_Orp1. Mean intensity values within each ROI were calculated under 405 nm and 488 nm excitation channels sequentially. The 405/488-nm intensity ratio for each ROI was calculated in Excel, and was compiled to generate the mean ratio for each brain sample.

To create false colour ratio images, maximal intensity projections were first converted from 16 to 32-bit format. ROIs were detected manually or automatically as described above. Image background (regions outside of ROIs) was cleared. A ratio image was generated by pixel by pixel division of 405 nm image over 488 nm image. Ratio images in false colour were generated in Image J using the 'fire' LookUp Table (LUT).

For ratiometric measurement of lipid peroxidation in LDs at the AL, maximal intensity projections were acquired from *z*-stack images in Image J. ROIs were manually selected to represent each neutral lipid droplet at the AL under the LipidTox Alexa 647 (deep red) channel. After applying ROIs to the 488nm (oxidized) and 561nm (non-oxidized) excitation channels, the intensity ratio of 488nm:561nm for each ROI was calculated in excel, and was compiled to generate the mean value for each brain sample. The mean value for each genotype group was normalized to the mean of control samples.

Images to be compared were collected using identical laser and detector settings. To compare protein expression level and cell numbers in fixed samples, images with same numbers of *z*-stacks were analysed. Sample size and number of replicates were described in the corresponding legends. Statistical analyses were performed with Prism version 7.05 (GraphPad Software). Statistical significance was calculated using Mann–Whitney test to compare means from two independent groups, or using Kruskal–Wallis test or Dunn's multiple comparisons test for multiple comparisons, as described in the figure legends. No statistical method was used to predetermine sample sizes. For *Ecc15* treatments, flies with the same sex, age and genotype were randomly assigned to control or experimental groups. Where cohorts of flies with defined sex, age and genotypes were compared, flies were randomly collected from breeding cages, sorted according to sex and genotype, and combined into cohorts. As all flies in a cohort were analysed, no randomization had to be performed in the data collection. No statistical methods were used to predetermine sample size.

Reporting summary

Further information on research design is available in the Nature Research Reporting Summary linked to this paper.

Data availability

The authors declare that the data supporting the findings of this study are available within the Article and its Supplementary Information. Raw sequencing reads and pre-processed sequence data for bulk RNA-seq files have been deposited in the Gene Expression Omnibus (GEO) under accession code GSE168530. Raw scRNA-seq reads and preprocessed sequence data have been deposited in the GEO under accession code GSE168572. Source data are provided with this paper.

Code availability

Analysis code for scRNA-seq datasets is available at https://github.com/Hongjie-Li/flyglia. *Drosophila* genome (version BDGP6) is available for download at https://aug2017.archive.ensembl.org/info/data/ftp/index.html. *Drosophila* genome (r6.10) is available for download at http://ftp.flybase.net/releases/. The published scRNA-seq datasets generated by the S. Aerts laboratory are available at https://scope.aertslab.org.

33. Hakim-Mishnaevski, K., Flint-Brodsly, N., Shklyar, B., Levy-Adam, F. & Kurant, E. Glial phagocytic receptors promote neuronal loss in adult drosophila brain. *Cell Rep*. **29**, 1438–1448.e3 (2019).
34. Albrecht, S. C., Barata, A. G., Grosshans, J., Teleman, A. A. & Dick, T. P. In vivo mapping of hydrogen peroxide and oxidized glutathione reveals chemical and regional specificity of redox homeostasis. *Cell Metab*. **14**, 819–829 (2011).
35. Li, H. et al. Classifying drosophila olfactory projection neuron subtypes by single-cell RNA sequencing. *Cell* **171**, 1206–1220.e22 (2017).
36. Anders, S. & Huber, W. Differential expression analysis for sequence count data. *Genome Biol*. **11**, R106 (2010).
37. Picelli, S. et al. Full-length RNA-seq from single cells using Smart-seq2. *Nat. Protocols* **9**, 171–181 (2014).
38. Dobin, A. et al. STAR: ultrafast universal RNA-seq aligner. *Bioinformatics* **29**, 15–21 (2013).
39. Anders, S., Pyl, P. T. & Huber, W. HTSeq—a Python framework to work with high-throughput sequencing data. *Bioinformatics* **31**, 166–169 (2015).
40. Ja, W. W. et al. Prandiology of *Drosophila* and the CAFE assay. *Proc. Natl Acad. Sci. USA* **104**, 8253–8256 (2007).

Acknowledgements We thank E. Bach, D. Bilder, S. Hou, M. Zeidler, N. Buchon, D. Ferrandon, L. O'Brien, M. A. Welte, M. Miura, C. S. Thummel and T. Dick for flies; M. Sagolla for the training in Yokogawa CSU-W1/Zeiss 3i Marianas spinning disk confocal microscope; the Genentech NGS technology core lab for the support with bulk RNA-seq; and I. C. Grunwald Kadow for the tips in olfactory T-maze assay. We acknowledge funding from the following grants: National Institutes of Health (NIH) R01AG057353 and Genentech, Inc (H.J.) NIH R00AG062746 (H.L.), NIH K99AG056680 (M.B.J.), NIH R56AG057304 (P.H.), NIH R01DC005982 (L.L.), Howard Hughes Medical Institute (L.L.), C. Zuckerberg Biohub (S.R.Q.) Cancer Prevention & Research Institute of Texas (H.L.). The funders had no role in study design, data collection and interpretation, or the decision to submit the work for publication.

Author contributions X.T.C. and H.J. designed all experiments. H.L. performed scRNA-seq experiments and analysis. L.L. and S.R.Q. provided resources and guidance for scRNA-seq

experiments. M.B.J., E.M. and P.H. contributed ideas and experiments to Fig. 1g and Extended Data Fig. 4a–d. J.B. contributed to glia sorting in Extended Data Fig. 7g. Y.L. performed bulk RNA sequencing in Extended Data Fig. 7. X.T.C. performed all other experiments and analysed the data. X.T.C. and H.J. wrote the manuscript with input from the other authors.

Competing interests X.T.C. is an employee of Genentech Inc., a Roche subsidiary. H.J., J.B. and Y.L. are employees and shareholders of Genentech Inc., a Roche subsidiary. M.B.J. is employee and shareholder of Gordian Biotechnology.

Additional information

Supplementary information The online version contains supplementary material available at https://doi.org/10.1038/s41586-021-03756-0.

Correspondence and requests for materials should be addressed to H.J.

Peer review information *Nature* thanks Matthew Moulton, Scott Pletcher and the other, anonymous, reviewer(s) for their contribution to the peer review of this work. Peer review reports are available.

Reprints and permissions information is available at http://www.nature.com/reprints.

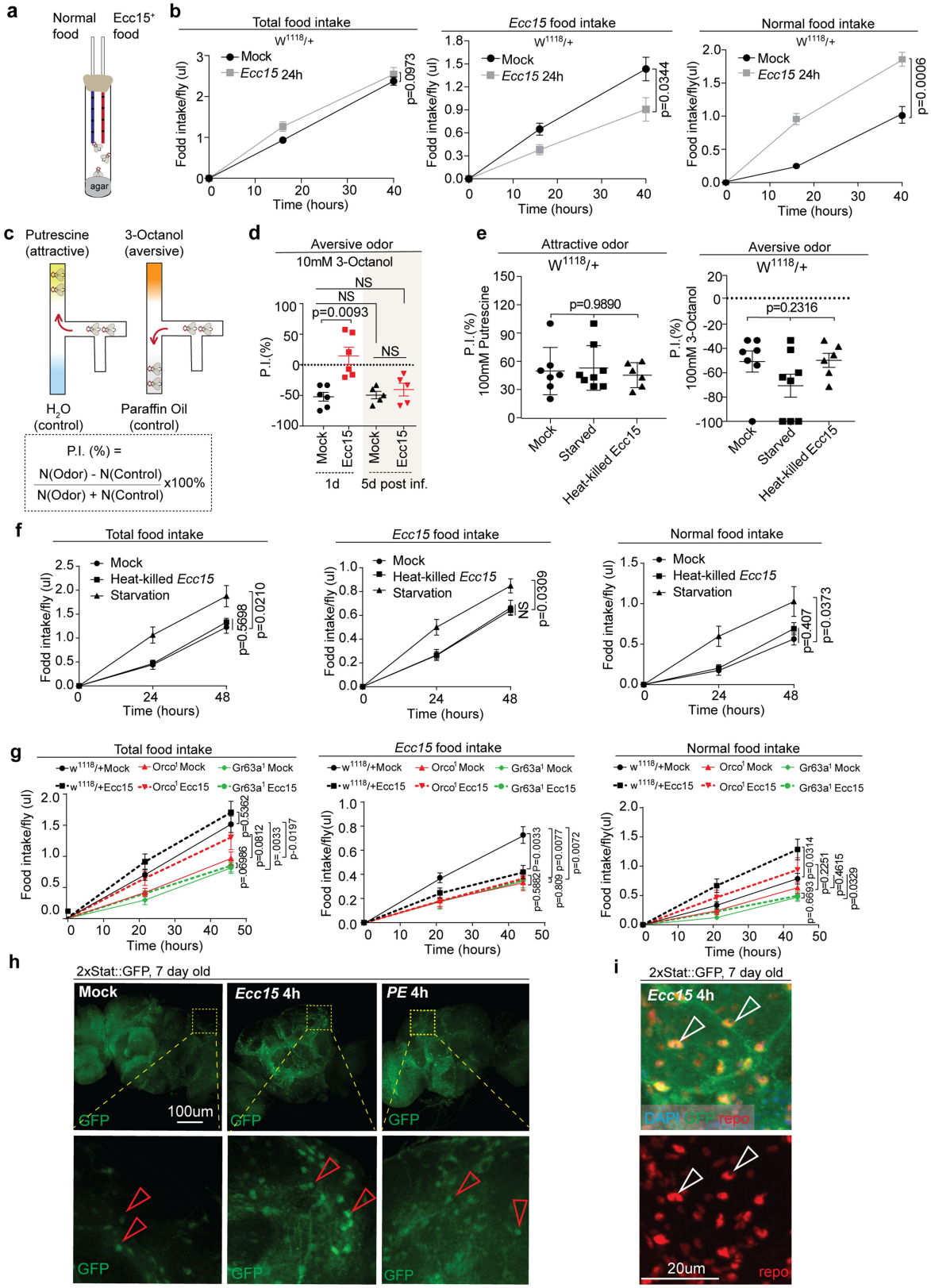

Extended Data Fig. 1 | See next page for caption.

Extended Data Fig. 1 | Orco and Gr63 odour receptors are required for infection-induced avoidance behaviours towards enteropathogens. **a**, Modified CAFE assay used. **b**, Intake of total food, *Ecc15* containing food and normal food for wild-type flies (w^{1118} × *OreR*) during homeostasis and 24 h after *Ecc15* infection respectively. **c**, Olfactory T-maze assay and calculation of preference index (P.I.). **d**, Preference index of young flies 24 h (1d) and 5 days (5d) after *Ecc15* infection towards aversive odour, respectively. **e**, Preference index of wild-type flies (w^{1118} × *OreR*) during homeostasis, infected with heat-killed *Ecc15* or starved on water for 24 h correspondingly. **f**, Intake of total food, *Ecc15*-containing food and normal food for flies in **e**. **g**, Intake of total food, *Ecc15*-containing food and normal food for wild-type flies (w^{1118} × *OreR*), $Gr63a^{1}$ flies, $Orco^{1}$ flies with or without *Ecc15* infection, respectively. **h**, **i**, Representative images of 2xSTAT::GFP expression in the central brain 4 h after *Ecc15* infection or *PE* infection, as determined by immunostaining. Anti-GFP antibody amplifies 2xSTAT::GFP signal. Anti-repo immunohistochemistry to label all glia in **i**. Number quantifications of $STAT^{+}$ cells per condition are shown in Fig. 1c. Data are mean and s.e.m. The sample size is as follows: $n = 7$ replicates (3 flies per cohort) per condition in **b**, $n = 5$ and 6 independently performed experiments for 1 and 5 days after infection, respectively, in **d**, $n = 7$, 8 and 6 independently performed experiments for mock, starved and infected flies with heat-killed *Ecc15* in **e**, $n = 10$ replicates (3 flies per cohort) per condition in **f**, $n = 7$, 10, 8, 9, 10 and 10 replicates (3 flies per cohort) for w^{1118} mock, w^{1118} *Ecc15*, $Orco^{1}$ mock, $Orco^{1}$ *Ecc15*, $Gr63a^{1}$ mock, $Gr63a^{1}$ *Ecc15* in **g**. Data shown in **f** and **g** are representative of two independently performed experiments, and those shown in **b**, **d**, **h** and **i** are representative of three separate experiments. *P* values in **b** and **g** from two-tailed Mann–Whitney test; *P* values in **d** and **f** from Dunn's multiple comparisons test; other *P* values from Kruskal–Wallis test. NS, not significant ($P > 0.9999$ in **d**, **f**).

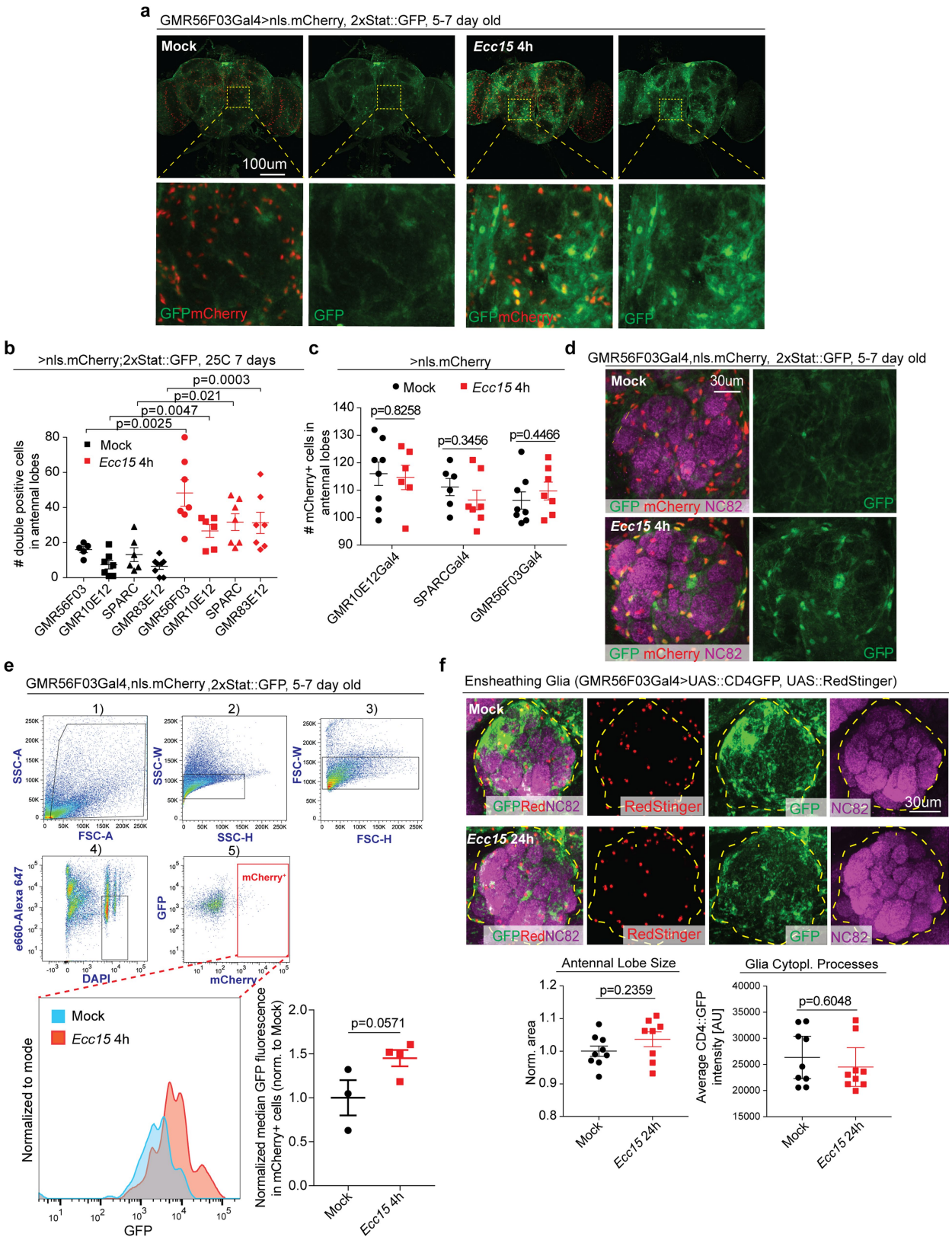

Extended Data Fig. 2 | See next page for caption.

Extended Data Fig. 2 | Infection does not influence numbers and the morphology of EG at the AL. a, **d**, Representative images of 2xSTAT::GFP expression in the EG (nls.mCherry$^+$ driven by GMR56F03::Gal4) in the central brain during homeostasis and 4 h after *Ecc15* infection. The AL region was magnified in **a** and additional images are shown in **d**. Anti-GFP antibody amplifies the 2xSTAT::GFP signal. Anti-NC82 antibody stained neuropils in **d**. **b**, Quantification of 2xSTAT::GFP reporter activity in the EG (nls.mCherry$^+$ in the presence of corresponding Gal4 drivers) during homeostasis and after *Ecc15* infection. Numbers of GFP$^+$ mCherry$^+$ cells from both ALs were quantified from 30-µm *z*-sections (2 µm each). Four different EG-specific Gal4 drivers were tested correspondingly. **c**, Quantification of EG numbers (nls.mCherry$^+$ driven by SPARC::Gal4, GMR10E12::Gal4 or GMR56F03::Gal4 respectively) at both ALs under mock and infected conditions. **e**, Histogram overlay of GFP fluorescence in mCherry$^+$ EG in the presence of GMR56F03::Gal4 under conditions as noted, measured by intracellular flow cytometry assay. The GFP fluorescence intensity level (logarithmic scale) is shown in the *x* axis; the number of events (normalized to its peak height, noted as normalized to modal) is shown on the *y* axis. Median fluorescence intensity of GFP in mCherry$^+$ EG under these conditions, was computed by FlowJo software and normalized to the median value of mock samples collected on the same day of measurement. mCherry$^+$ EG were sorted by the following gates: (1) forward versus side scatter (FSC versus SSC); (2) side scatter height versus width (SSC-H vs SSC-W); (3) forward scatter height versus width (FSC-H versus FSC-W); (4) fixable viability dye (eFluor 660 to label dead cells before fixation) versus DAPI (labelling nuclei to exclude debris); (5) GFP versus mCherry fluorescence channel (GFP versus mCherry). **f**, Representative images showing EG morphology at the AL from control and infected flies. EG nuclei were labelled by RedStinger, and cellular processes were labelled by CD4::GFP. Neuropils were labelled by an anti-NC82 antibody . Representative images were generated from 7-µm *z*-sections (1 µm each) after performing maximal intensity projection. Average intensity levels of CD4::GFP were quantified from 20-µm *z*-stack confocal images after maximal intensity projection. AL sizes were quantified and normalized to the mean value of mock flies. Data are mean and s.e.m. The sample size is as follows: $n = 5, 7, 6, 8, 7, 6, 7$ and 7 brains per condition (from left to right) in **b**, $n = 8, 6, 6, 7, 8$ and 7 brains per condition (from left to right) in **c**, $n = 97, 135$ and 822 mCherry$^+$ cells from mock flies and $n = 123, 91, 145$ and 163 mCherry$^+$ cells from infected flies in **e**, $n = 9$ and 8 brains for mock and *Ecc15* flies in **f** (left), $n = 9$ brains per condition in **f** (right). Data in **a** and **d** are representative of three independently performed experiments; data shown in **b**, **c**, **e** and **f** are representative of two independently performed experiments. *P* values in **e** from one-tailed Mann–Whitney test; other *P* values from two-tailed Mann–Whitney test.

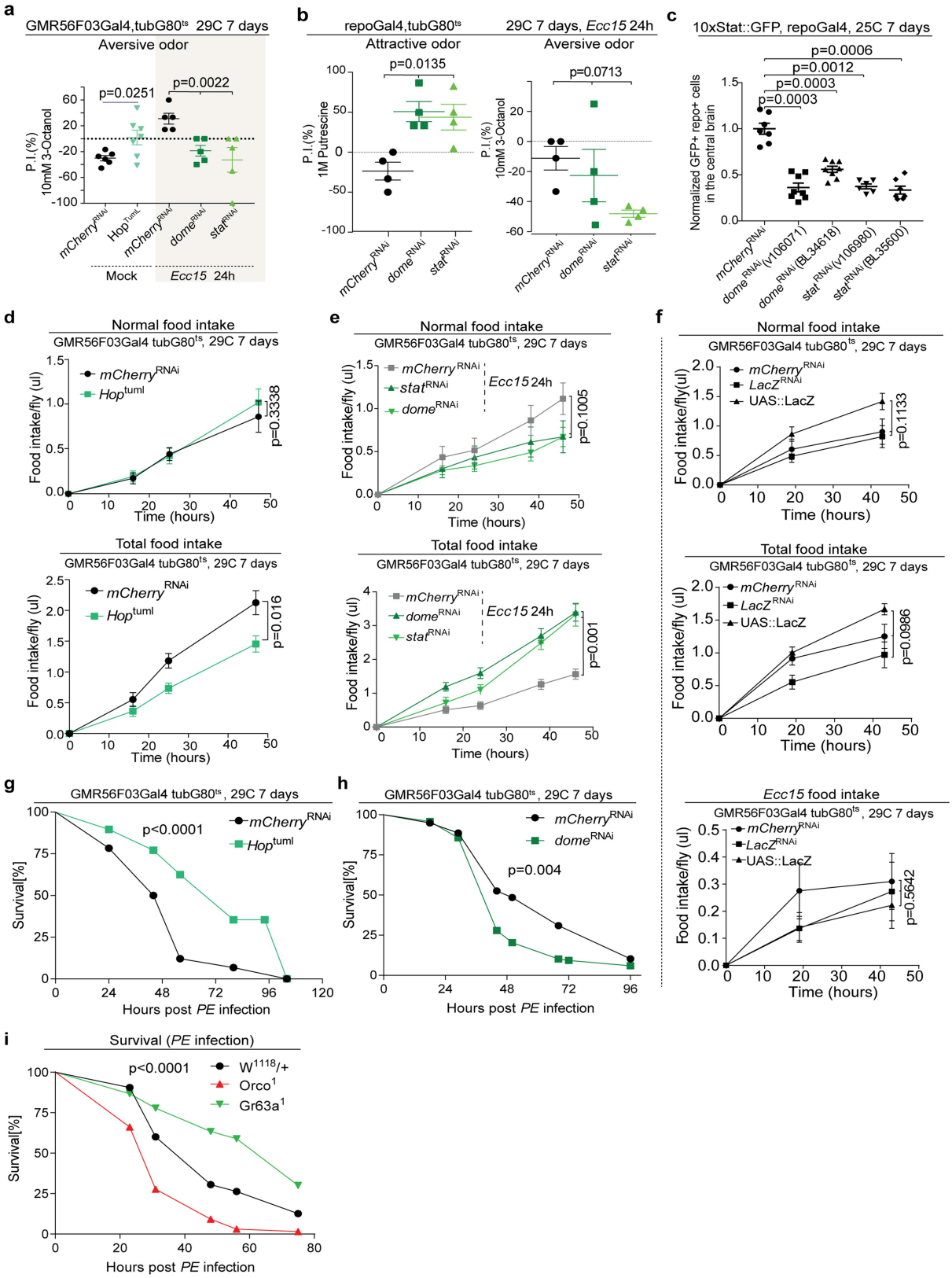

Extended Data Fig. 3 | See next page for caption.

Extended Data Fig. 3 | JAK–STAT signalling in EG promotes avoidance behaviour against *Ecc15*, yet increasing host survival upon acute infection. **a**, Preference index of young flies with indicated JAK–STAT perturbation in the EG. RNAi constructs were expressed in the EG for 7 days by shifting flies to 29 °C (restrictive temperature for Gal80^{ts}). Flies were exposed to *Ecc15* for 24 h. **b**, Preference index of young infected flies expressing *mCherry*^{RNAi}, *dome*^{RNAi} or *stat*^{RNAi} in all glia (repo::Gal4;tubG80^{ts}), measured by T-maze assay. **c**, Quantification of STAT::GFP activity in the glia of flies after *dome*^{RNAi} or *stat*^{RNAi} knockdown in all glia (repo::Gal4; 10xSTAT::GFP), to confirm knockdown efficiency for various RNAi lines that target Dome or STAT, respectively. **d**, **e**, Total food intake and normal food intake of flies overexpressing *hop*^{tuml} (**d**) and of infected flies after knockdown of *dome* and *stat* (**e**) in EG (driven by GMR56F03::Gal4;tubG80^{ts}), measured by CAFE assay. **f**, Intake of total food, *Ecc15*-containing food and normal food for flies expressing *mCherry*^{RNAi}, *LacZ*^{RNAi} and UAS::LacZ in the EG during homeostasis. **g**, **h**, Survival curve of flies overexpressing *hop*^{tuml} (**g**) or knocking down *dome* (**h**) in the EG after continuous *PE* infection. **i**, Survival curves of wild-type flies (w^{1118} × *OreR*), *Gr63a*^{1} flies, *Orco*^{1} flies after continuous *PE* infection. Data are mean and s.e.m. The sample size is as follows: n = 6, 7, 5, 5 and 5 independently performed experiments per condition (from left to right) in **a**, n = 4 independently performed experiments per condition in **b**, n = 7, 8, 8, 6 and 7 brains per condition (from left to right) in **c**, n = 8 and 9 replicates (3 flies per cohort) for *mCherry*^{RNAi} and *hop*^{tuml}, respectively in **d**, n = 6, 8 and 7 replicates (3 flies per cohort) for *mCherry*^{RNAi}, *dome*^{RNAi} and *stat*^{RNAi} in **e**, n = 8 replicates per condition (3 flies per cohort) for **f**, n = 74 and 96 flies for *mCherry*^{RNAi} and *hop*^{tuml}, respectively, for **g**, n = 97 and 118 flies for *mCherry*^{RNAi} and *dome*^{RNAi}, respectively, for **h**, n = 101, 63 and 90 flies for wild-type flies (w^{1118} × *OreR*), *Orco*^{1}, *Gr63a*^{1} flies for **i**. Data in **d**, **e**, **g**, **h** are representative of three independently performed experiments; data shown in **c**, **f** and **i** are representative of two independently performed experiments. *P* values from two-tailed Mann–Whitney test in **a** (*mCherry*^{RNAi} compared with *hop*^{tuml}), **c**, **d**; *P* values from log-rank test in **g**–**i**; other *P* values from Kruskal–Wallis test.

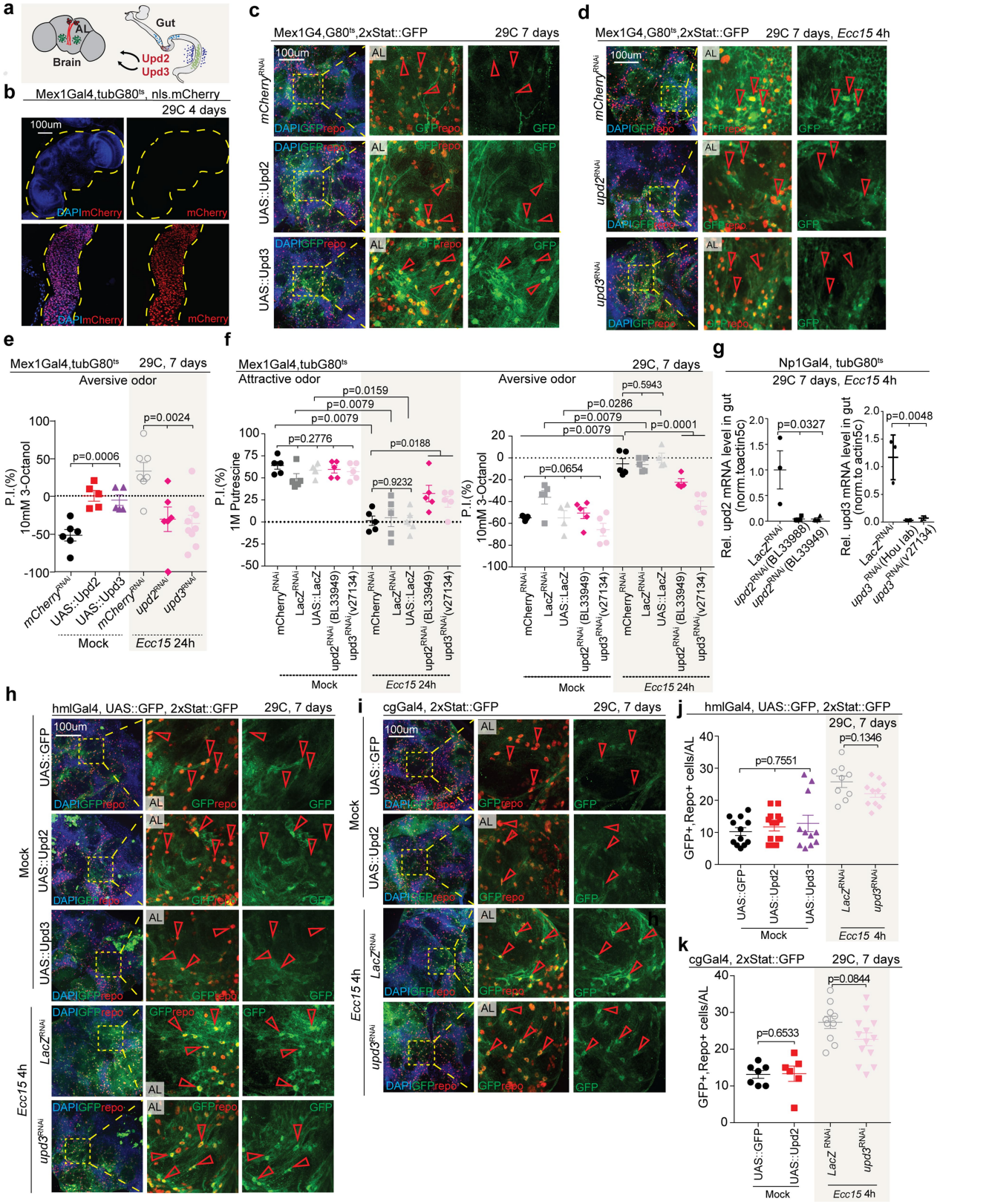

Extended Data Fig. 4 | See next page for caption.

Extended Data Fig. 4 | Gut-derived Upd2 and Upd3 are sufficient and required for infection-induced STAT activation in the glia. a, Gut-derived Upd proteins and their possible effect on the AL. **b**, Glial expression of nuclear mCherry driven by Mex1::Gal4 in the gut and brain of adult flies. **c**, **d**, Activity of 2xSTAT::GFP reporter in the central brain of flies overexpressing *upd2*, *upd3* in enterocytes, driven by Mex1::Gal4;tubG80^{ts}, during homeostasis (**c**) and of infected flies loss of *upd2*, *upd3* in enterocytes (**d**). Representative images were generated from 30-µm *z*-sections, and the AL region was magnified. Numbers of GFP$^+$, repo$^+$ glia per AL were quantified in Fig. 1g. **e**, **f**, Preference index of flies expressing *mCherry*^{RNAi}, UAS::LacZ, *LacZ*^{RNAi}, UAS::upd2, UAS::upd3 and RNAi lines targeting *upd2* or *upd3* in enterocytes with or without *Ecc15* infection. **g**, qPCR analysis confirming the knockdown efficiency of multiple RNAi lines targeting *upd2* or *upd3* correspondingly. **h**, **j**, Activity of 2xSTAT::GFP reporter in the central brain of flies overexpressing *upd2* or *upd3* in haemocytes (driven by hm1::Gal4) during homeostasis and of infected flies loss of *upd3* in haemocytes. Numbers of GFP$^+$ repo$^+$ cells per AL were quantified from 30-µm *z*-sections in **j**, and the AL region was magnified. **i**, **k**, Activity of 2xSTAT::GFP reporter in the central brain of flies overexpressing *upd2* in fatbody (driven by cg::Gal4) during homeostasis and of infected flies loss of *upd3* in fatbody. Numbers of GFP$^+$ repo$^+$ cells per AL were quantified from 30-µm *z*-sections in **k**, and the AL region was zoomed in. Data are mean and s.e.m. The sample size is as follows: $n = 6, 5, 5, 7, 6$ and 9 independently performed experiments per condition (from left to right) in **e**, $n = 4$ or 5 independently performed experiments per condition in **f**, $n = 3, 4$ and 4 biological replicates per condition (from left to right) in **g** (left), $n = 3, 4$ and 2 biological replicates per condition (from left to right) in **g** (right), $n = 12, 14, 11, 9$ and 11 brains per condition (from left to right) in **j**, $n = 7, 6, 10$ and 13 brains per condition (from left to right) in **k**. Data in **c** and **d** are representative of three independently performed experiments; data shown in **b**, **g**–**k** are representative of two independently performed experiments. *P* values from two-tailed Mann–Whitney test in **f**, **j** and **k** when comparing two groups; other *P* values from Kruskal–Wallis test.

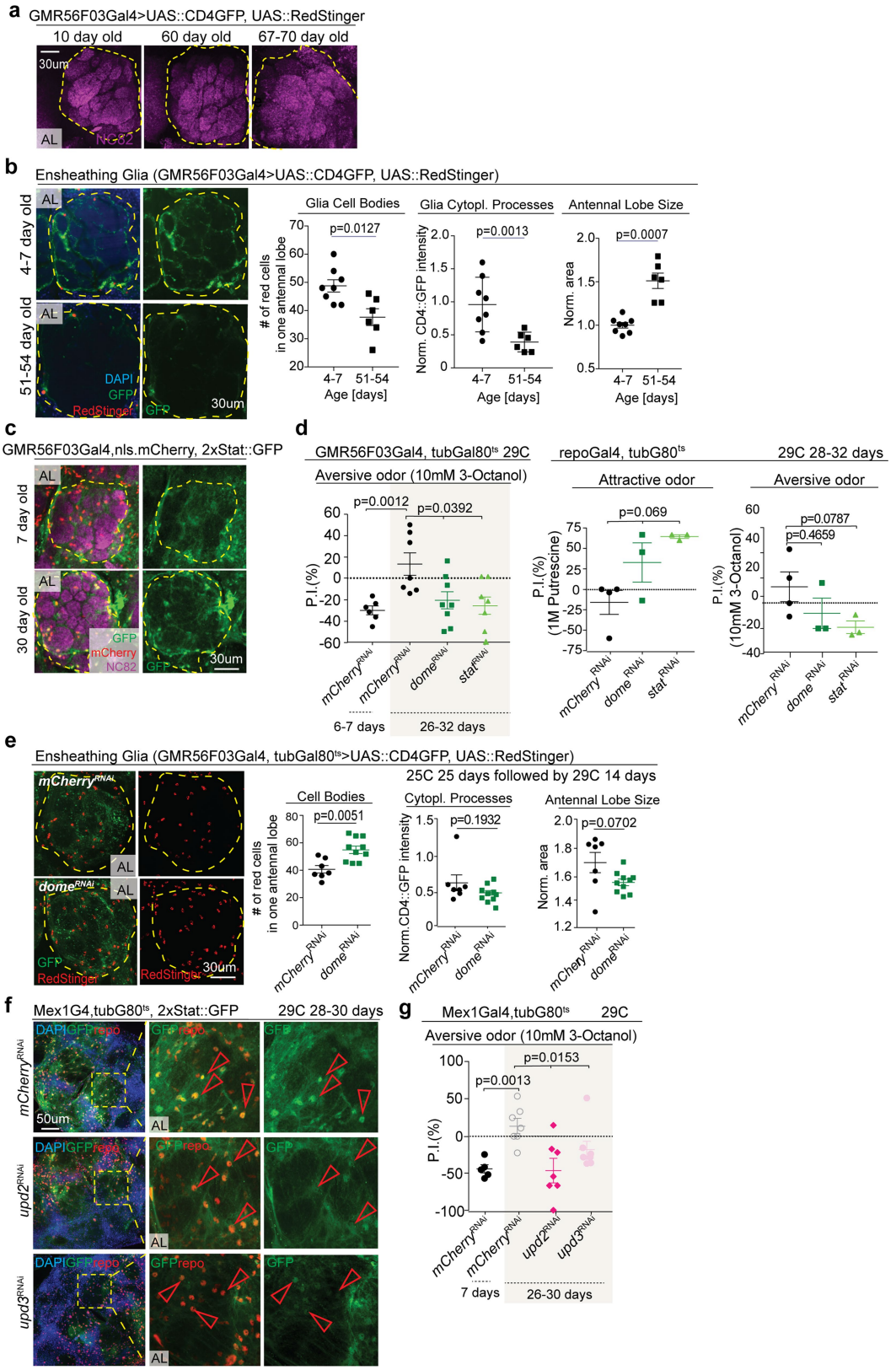

Extended Data Fig. 5 | See next page for caption.

Extended Data Fig. 5 | Chronic activation of JAK–STAT signalling in EG drives the decline of EG numbers at the AL during ageing. a, Representative images of glomerular compartments at the AL from young and old flies. Confocal images were generated from 20-µm *z*-sections (1 µm each) after performing maximal intensity projection. Neuropils labelled by anti-NC82 antibody. **b**, Representative single *z*-section images showing EG morphology at the AL from young and old flies. EG nuclei were labelled by RedStinger driven by GMR56F03::Gal4, and cellular processes were labelled by CD4::GFP. Average intensity levels of CD4::GFP and AL sizes were quantified from 20-µm *z*-stack confocal images after maximal intensity projection. AL sizes were quantified and normalized to the mean values of young flies. **c**, Representative images of 2xSTAT::GFP reporter activity in EG (nls.mCherry^{+} driven by GMR56F03::Gal4) at the AL from young and old flies. Images were generated from 20-µm *z*-sections (1 µm each) after performing maximal intensity projection. **d**, Preference index of young flies expressing *mCherry*^{RNAi} in EG (GMR56F03::Gal4), old flies expressing *mCherry*^{RNAi}, *dome*^{RNAi} or *stat*^{RNAi} in EG or all glia (repo::Gal4), measured by T-maze assay. **e**, Representative images showing EG morphology at the AL from old flies with or without *dome* knockdown. EG nuclei were labelled by RedStinger in the presence of GMR56F03::Gal4;tubG80^{ts}, while cellular processes were labelled by CD4::GFP. Average intensity levels of CD4::GFP and numbers of RedStinger^{+} cells per AL were quantified. AL sizes were quantified and normalized to the mean value of old control flies. Flies were aged at 25 °C for 14 days followed by 29 °C for 14 days to induce *dome*^{RNAi} expression. **f**, Representative images showing the activity of 2xSTAT::GFP reporter in the central brain of old flies knocking down *upd2* or *upd3* in enterocytes, driven by Mex1::Gal4;tubG80^{ts}. Representative images were generated from 30-µm *z*-sections, and the AL region was magnified. **g**, Preference index of young flies expressing *mCherry*^{RNAi} and old flies expressing *mCherry*^{RNAi}, *Upd2*^{RNAi} or *Upd3*^{RNAi} in enterocytes, driven by Mex1::Gal4;tubG80^{ts}. Data are mean and s.e.m. The sample size is as follows: $n = 8$ and 6 brains for young and old conditions, respectively, in **b**, $n = 6, 7, 8$ and 7 independently performed experiments for young *mCherry*^{RNAi}, old *mCherry*^{RNAi}, *dome*^{RNAi} and *stat*^{RNAi} correspondingly in **d** (left), $n = 4, 3$ and 3 independently performed experiments for old *mCherry*^{RNAi}, *dome*^{RNAi} and *stat*^{RNAi} correspondingly in **d** (middle and right), $n = 7$ and 10 brains for *mCherry*^{RNAi}, *dome*^{RNAi}, respectively, in **e**, $n = 5, 7, 7$ and 7 independently performed experiments for young *mCherry*^{RNAi}, old *mCherry*^{RNAi}, *Upd2*^{RNAi} and *Upd3*^{RNAi}, respectively, in **g**. Data in **a**–**c**, **f** are representative of two independently performed experiments; data in **e** are representative of three independently performed experiments. *P* values from two-tailed Mann–Whitney test in **b**, **d** (when comparing young and old *mCherry*^{RNAi}), **e**, **g** (when comparing young and old *mCherry*^{RNAi}); *P* values from Dunn's multiple comparisons test in **d** (right); other *P* values from Kruskal–Wallis test.

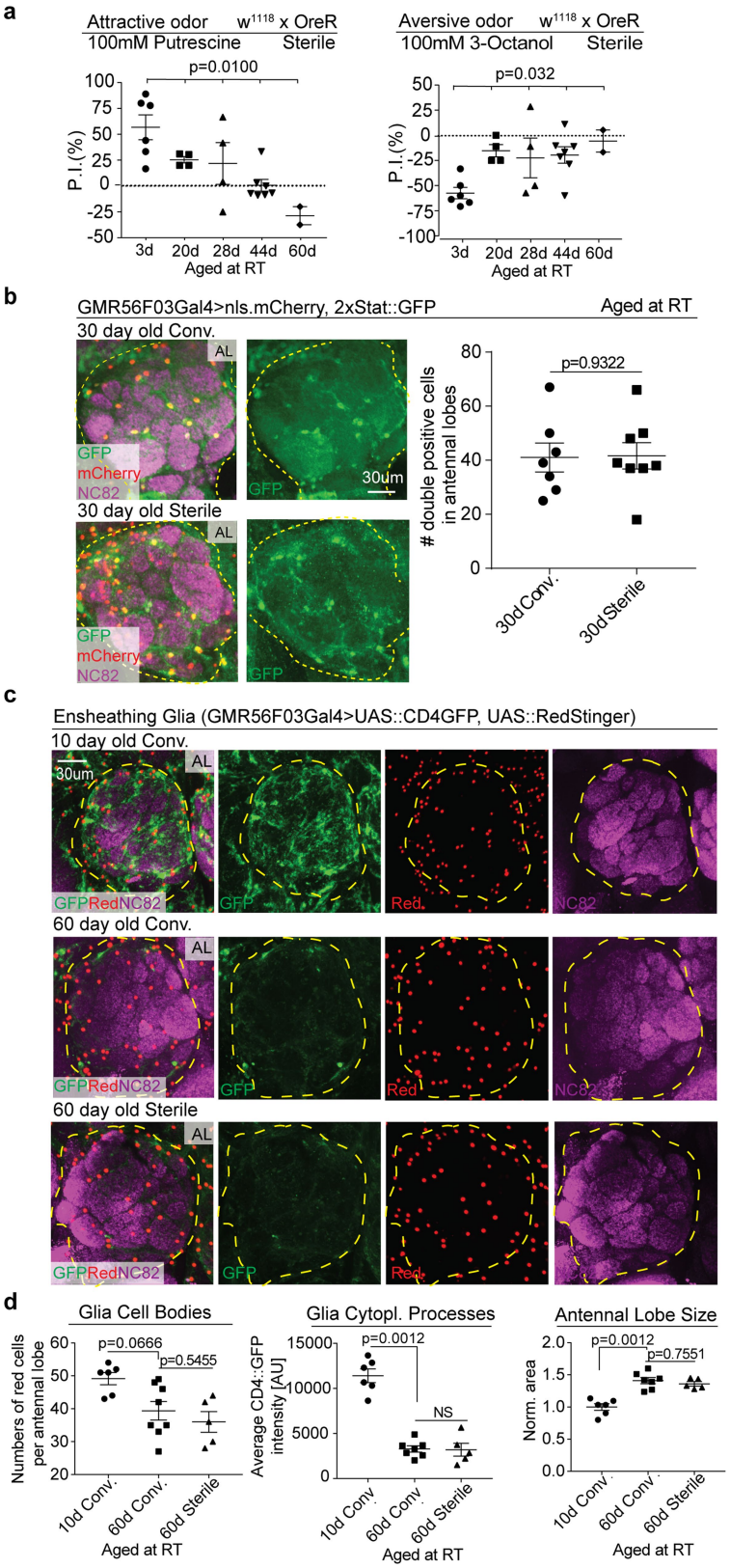

Extended Data Fig. 6 | See next page for caption.

Extended Data Fig. 6 | Age-related decline of olfaction sensitivity and morphological decays of EG are independent from microbiota. **a**, Preference index of germ-free wild-type flies ($w^{1118} \times OreR$) during ageing, measured by T-maze assay. **b**, Representative images of 2xSTAT::GFP reporter activity in the EG at the AL from conventionally-reared or germ-free old flies. EG nuclei were labelled by nls.mCherry in the presence of GMR56F03::Gal4 driver. Anti-GFP antibody amplified 2xSTAT::GFP signal. Anti-NC82 antibody labelled neuropils. Confocal images were generated from 20-µm *z*-sections after performing maximal intensity projection. Flies were aged at room temperature. **c**, **d**, Representative images showing EG morphology at the AL from young and old flies that were conventionally reared and from old germ-free flies, respectively. EG nuclei were labelled by RedStinger in the presence of GMR56F03::Gal4, and cellular processes were labelled by CD4::GFP. Neuropils were labelled by anti-NC82 antibody . Images were generated from 20-µm *z*-sections after performing maximal intensity projection. Average intensity levels of CD4::GFP and numbers of RedStinger$^+$ cells per AL were quantified in **d**. AL sizes were quantified and normalized to the mean value of young conventionally reared animals in **d**. Flies were aged at room temperature. Data are mean and s.e.m. The sample size is as follows: $n = 6, 4, 4, 7$ and 2 independently performed experiments per condition (from left to right) in **a**, $n = 7$ and 8 brains for 30-day conventional and 30-ayd sterile conditions, respectively, in **b**, $n = 6, 8$ and 5 brains per condition (from left to right) in **d** (left), $n = 6, 7$ and 5 brains per condition (from left to right) in **d** (middle and right). Data in **b**–**d** are representative of two independently performed experiments. *P* values from Kruskal–Wallis test in **a**; other *P* values from two-tailed Mann–Whitney test.

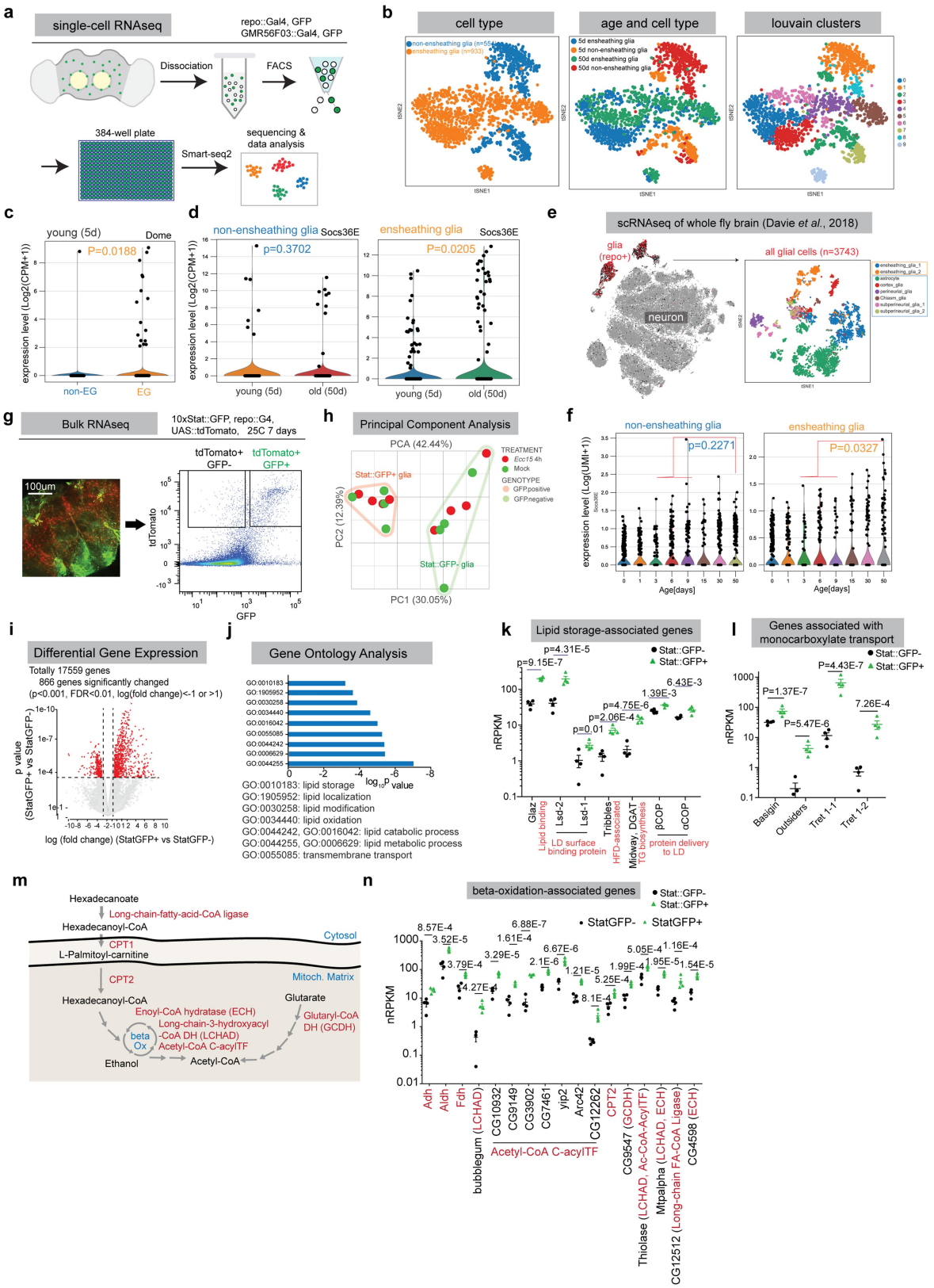

Extended Data Figure 7 | See next page for caption.

Extended Data Figure 7 | JAK–STAT signalling regulates glial lipid metabolism. a, Workflow of scRNA-seq using plate-based Smart-seq2. FACS, fluorescence-activated cell sorting. Four groups of glia were sequenced: 5 and 50 day all glia (GFP^+, driven by rep::Gal4); 5 and 50 day EG (GFP^+, driven by GMR56F03::Gal4). **b**, Visualization of glial cells using *t*-SNE plots. Cells were coloured according to cell types, ages and Louvain clusters with default resolution. Non-EG were curated from all $repo^+$ glia with EG ($GMR56F03::Gal4^+$) removed (Methods). EG and non-EG were readily separated into different clusters (left and middle). In total, 10 clusters were formed from these glia (right), suggesting the heterogeneity of glial population. **c**, Violin plot showing expression levels of *dome* in non-EG and EG. For both EG and non-EG, cells were combined from young and old flies. In non-EG, *dome* expression was barely detected except in one cell. In EG, a subset of cells showed high expression of *dome*. **d**, Violin plots showing expression levels of *Socs36E* in young and old non-EG (left) and EG (right) respectively. **e**, Visualization of all annotated glial cells from a previously published whole fly brain scRNA-seq dataset[22] using a *t*-SNE plot. scRNA-seq was performed using droplet-based 10x Genomics platform. Glia are in red ($repo^+$), and neurons are in grey. Two subsets of EG (in orange box) and six subsets of non-EG (in blue box) are annotated. **f**, Violin plots showing expression levels of *Socs36E* in non-EG and EG at eight different ages. Cells from 3-, 6- and 9-day-old flies were combined as young samples, and compared with cells from 50-day-old flies (old). **g**, Gating strategy for sorting $STAT::GFP^+$ glia and $STAT::GFP^-$ glia from the central brain of young mock or young infected (4-h *Ecc15* infection) flies overexpressing tdTomato in all glia (repo::Gal4) while expressing 10xSTAT::GFP reporter. **h**, Visualization of gene expression variation between $STAT::GFP^+$ glia and $STAT::GFP^-$ glia by PCA plot. Each dot represents a sample replicate independently collected from a cohort of 100 flies. Samples with the same genotype were grouped together, and samples with different treatments were coloured separately. **i**, Volcano plot displaying differentially expressed genes between $STAT::GFP^+$ glia and $STAT::GFP^-$ glia (highlighted in red) under homeostatic conditions, using a cut-off of twofold change, $P < 0.001$, FDR < 0.01. **j**, Gene Ontology analysis of significantly upregulated genes in $STAT::GFP^+$ glia during homeostasis. **k**, Lipid storage-associated genes were significantly upregulated in $STAT::GFP^+$ glia during homeostasis. Reads per kilobase per normalized million mapped reads (nRPKM) values of each gene in $STAT::GFP^+$ glia and $STAT::GFP^-$ glia are shown correspondingly. **l**, Genes involved in monocarboxylate transport were significantly upregulated in $STAT::GFP^+$ glia during homeostasis. nRPKM values of each gene in $STAT::GFP^+$ glia and $STAT::GFP^-$ glia are shown correspondingly. **m**, Schematic demonstrating mitochondrial fatty acid β-oxidation. **n**, Genes involved in fatty acid β-oxidation that were significantly upregulated in $STAT::GFP^+$ glia during homeostasis. nRPKM values of each gene in $STAT::GFP^+$ glia and $STAT::GFP^-$ glia are shown correspondingly. Data are mean and s.e.m. The sample size is as follows: $n = 4$ replicates per condition (each replicate was independently pooled from 100 flies on different days) in **g**–**n**. *P* values in **k**, **l** and **n** were calculated by Partek Flow; *P* values in **c**, **d** and **f** from one-tailed Student's *t*-test.

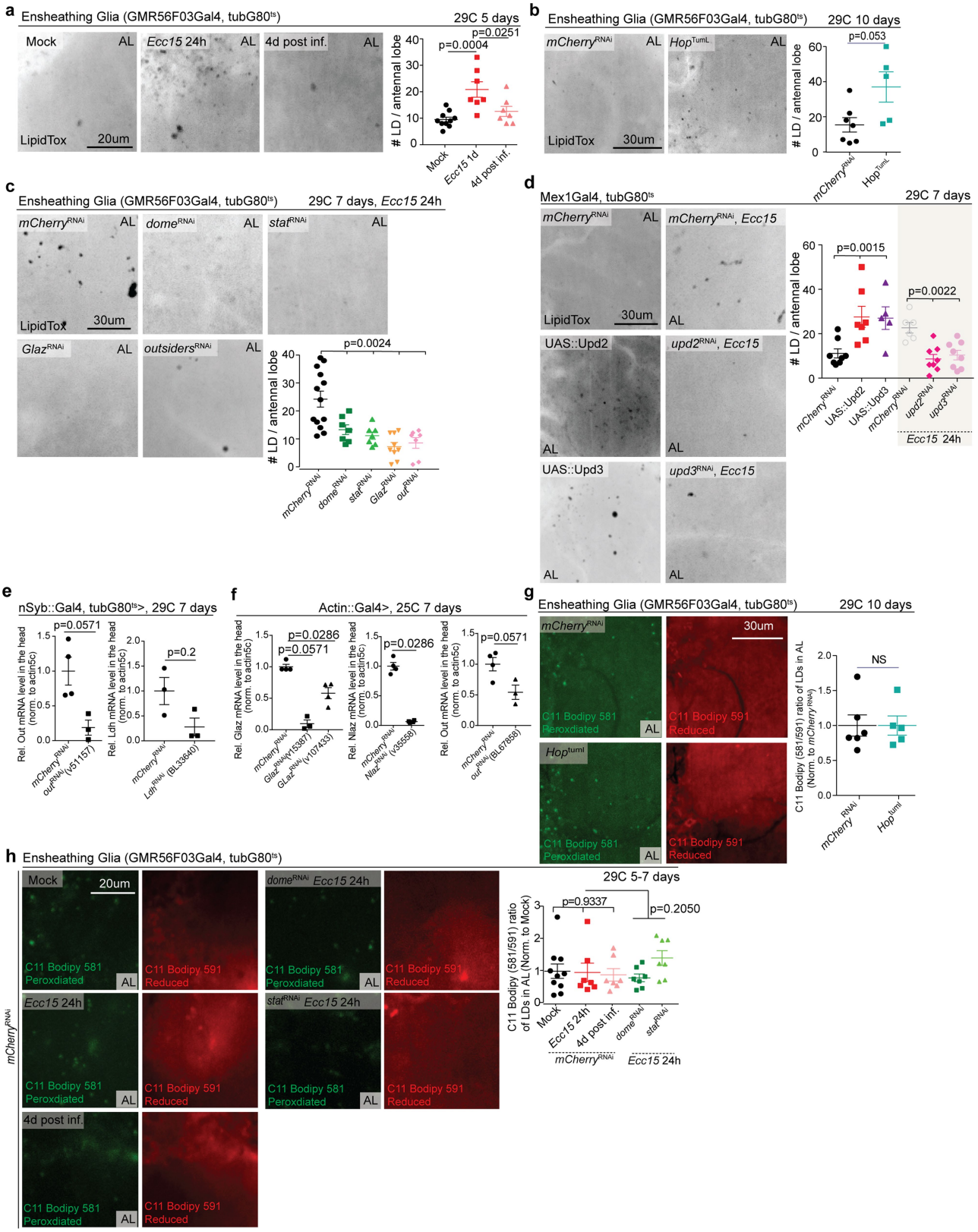

Extended Data Fig. 8 | See next page for caption.

Extended Data Fig. 8 | JAK–STAT signalling regulates LD accumulation via *GLaz* and *out* after infection, with no influence on lipid peroxidation. **a**, Immunostaining detecting LDs at the AL from young flies during homeostasis, 24 h after *Ecc15* infection, or 4 days after infection, using LipidTox deep red probes. LD numbers per AL were quantified. **b**, **c**, Immunostaining detecting LDs at the AL from young flies overexpressing $mCherry^{RNAi}$ or hop^{tuml} in EG (driven by GMR56F03::Gal4;tubG80^{ts}) during homeostasis (**b**), and from infected flies knocking down *dome*, *stat*, *GLaz* or *out* in EG (**c**). LD numbers per AL were quantified. **d**, Immunostaining detecting LDs at the AL from young flies overexpressing Upd cytokines in enterocytes, driven by Mex1::Gal4;tubG80^{ts}, during homeostasis, and from infected flies knocking down Upd cytokines in enterocytes. LD numbers per AL were quantified. **e**, **f**, qPCR analysis confirming the knockdown efficiency of several RNAi lines targeting *out*, *GLaz*, *NLaz* and *Ldh*, respectively. **g**, **h**, Representative images showing lipid peroxidation in LDs at the AL from young flies expressing $mCherry^{RNAi}$ or hop^{tuml} in the EG (driven by GMR56F03::Gal4;tubG80^{ts}) during homeostasis (**g**), from young mock flies, infected flies or 4 days after *Ecc15* infection (**h**), and from infected flies knocking down *dome* or *stat* in the EG (**h**). Lipid peroxidation levels of LDs for each sample were measured as the mean 488/561 nm intensity ratios in LDs. The ratios were normalized to the mean value of corresponding control samples. Data are mean and s.e.m. The sample size is as follows: $n = 10$, 7 and 7 brains per condition (from left to right) in **a**, $n = 7$ and 5 brains for $mCherry^{RNAi}$ and hop^{tuml}, respectively, in **b**, $n = 13$, 7, 7, 9 and 7 brains per condition for $mCherry^{RNAi}$, $dome^{RNAi}$, $stat^{RNAi}$, $GLaz^{RNAi}$ and out^{RNAi} in **c**, $n = 8$, 7, 5, 6, 8 and 8 brains per condition (from left to right) in **d**, $n = 4$ and 3 biological replicates for $mCherry^{RNAi}$ and out^{RNAi} in **e** (left), $n = 3$ biological replicates for $mCherry^{RNAi}$ and Ldh^{RNAi} in **e** (right), $n = 4$, 3, 4, 4, 4, 4 and 3 biological replicates per condition (from left to right) in **f**, $n = 6$ and 5 brains $mCherry^{RNAi}$ and hop^{tuml} in **g**, $n = 10$, 7, 7, 7 and 7 brains per condition (from left to right) in **h**. Images in **a**–**e**, **h** were generated from 20-μm *z*-sections (1-μm each) after performing maximal intensity projection. Data in **a**–**d**, **g**, **h** are representative of three independently performed experiments; data shown in **e** and **f** are representative of two separate experiments. *P* values in **a**, **b**, **e**–**g** from two-tailed Mann–Whitney test; other *P* values from Kruskal–Wallis test. NS, not significant ($P > 0.9999$ in **g**).

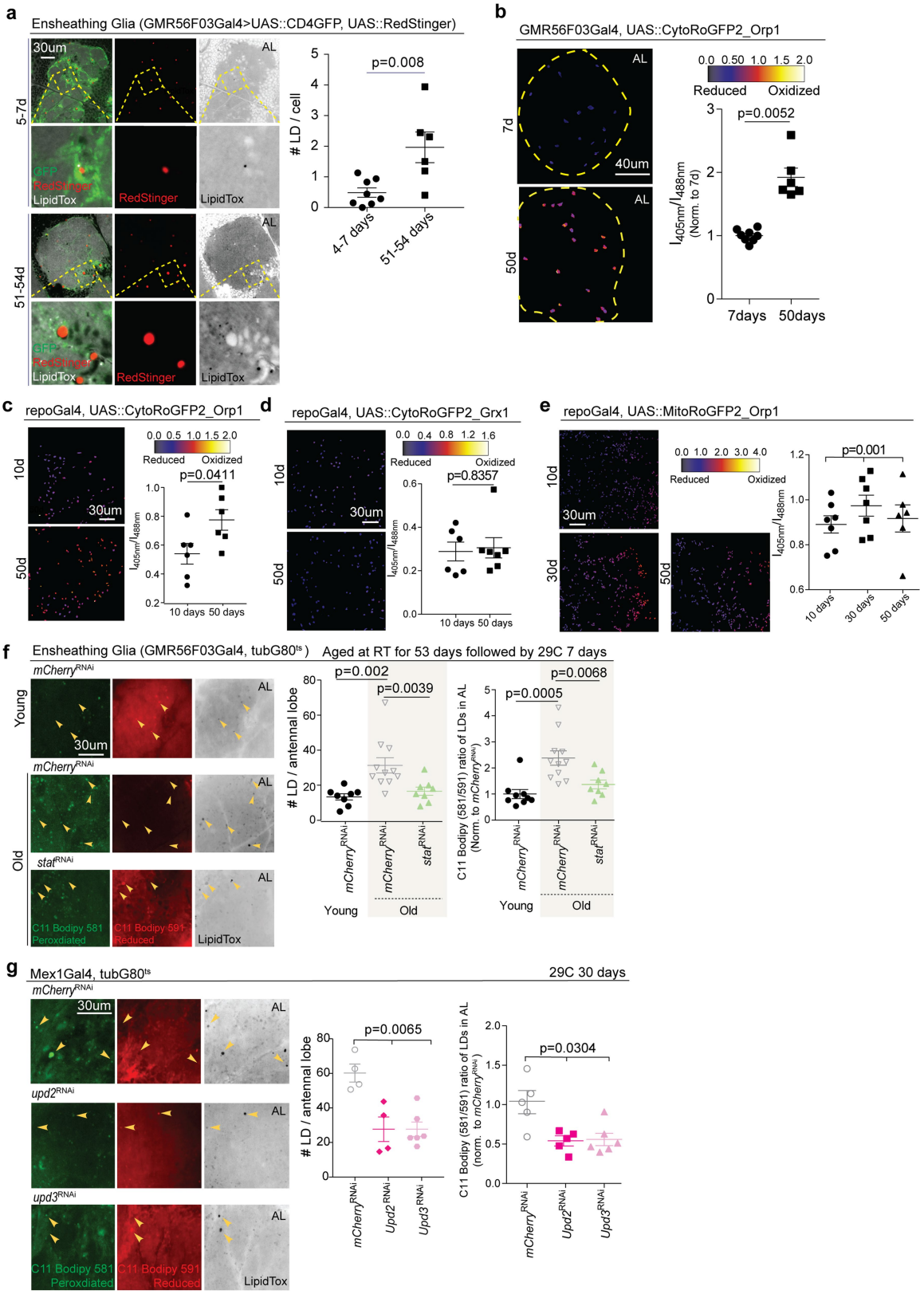

Extended Data Fig. 9 | See next page for caption.

Extended Data Fig. 9 | Deactivation of JAK–STAT signalling alleviates lipid toxicity during ageing, thus rescuing the age-related decline of ensheathing glia numbers. a, Immunostaining detecting LDs in EG (RedStinger^{+}, CD4::GFP^{+}) at the AL of young (5–7 day old) and old (51–54 day old) flies, using LipidTox deep red probes. LD numbers per glia were quantified. **b**, Cytosolic H_2O_2 levels in EG at the AL from young (7 day old) and old (50 day old) flies, measured as the mean 405/488 nm intensity ratio. The ratios for old flies were normalized to the mean value for young flies. **c**–**e**, Levels of cytosolic H_2O_2 (**c**), cytosolic glutathione redox potential (**d**) and mitochondrial H_2O_2 (**e**) in all glia (driven by repo::Gal4) from young and old flies, measured as the mean 405/488 nm intensity ratios for corresponding ROS sensors. **f**, Representative images showing lipid peroxidation in LDs at the AL from young flies expressing *mCherry*^{RNAi} in the EG (driven by GMR56F03::Gal4;tubG80^{ts}) and from old flies expressing *mCherry*^{RNAi} or *stat*^{RNAi} in the EG. LD numbers per AL were quantified. Lipid peroxidation levels of LDs for each sample were measured as the mean 488/561 nm intensity ratio. The ratios were normalized to the mean value of young control samples. Flies were aged at room temperature before being transferred to 29 °C for 7 days. **g**, Representative images showing lipid peroxidation in LDs at the AL from old flies after loss of *upd2* or *upd3* in enterocytes driven by Mex1::Gal4;tubG80^{ts}. LD numbers per AL were quantified. Lipid peroxidation levels of LDs for each sample were measured as the mean 488/561 nm intensity ratio. The ratios were normalized to the mean value of old control samples. Data are mean and s.e.m. The sample size is as follows: $n = 8$ and 6 brains for young and old conditions correspondingly in **a** and **b**, $n = 6$ brains per condition in **c**, $n = 6$ and 7 brains for young and old conditions correspondingly in **d**, $n = 7$, 7 and 6 brains per condition (from left to right) in **e**, $n = 8$, 11 and 8 brains per condition (from left to right) correspondingly in **f** (left), $n = 9$, 11 and 8 brains per condition (from left to right) correspondingly in **f** (right), $n = 4$, 4 and 6 brains per condition (from left to right) in **g** (left), $n = 5$, 5 and 6 brains per condition (from left to right) in **g** (right). Images in **a**–**g** were generated from 20-µm *z*-sections (1-µm each) after performing maximal intensity projection. Data in **a**–**e** are representative of two independently performed experiments, and those in **f** and **g** are representative of three separate experiments. *P* values in **a**–**d**, **f** from two-tailed Mann–Whitney test; other *P* values from Kruskal–Wallis test.

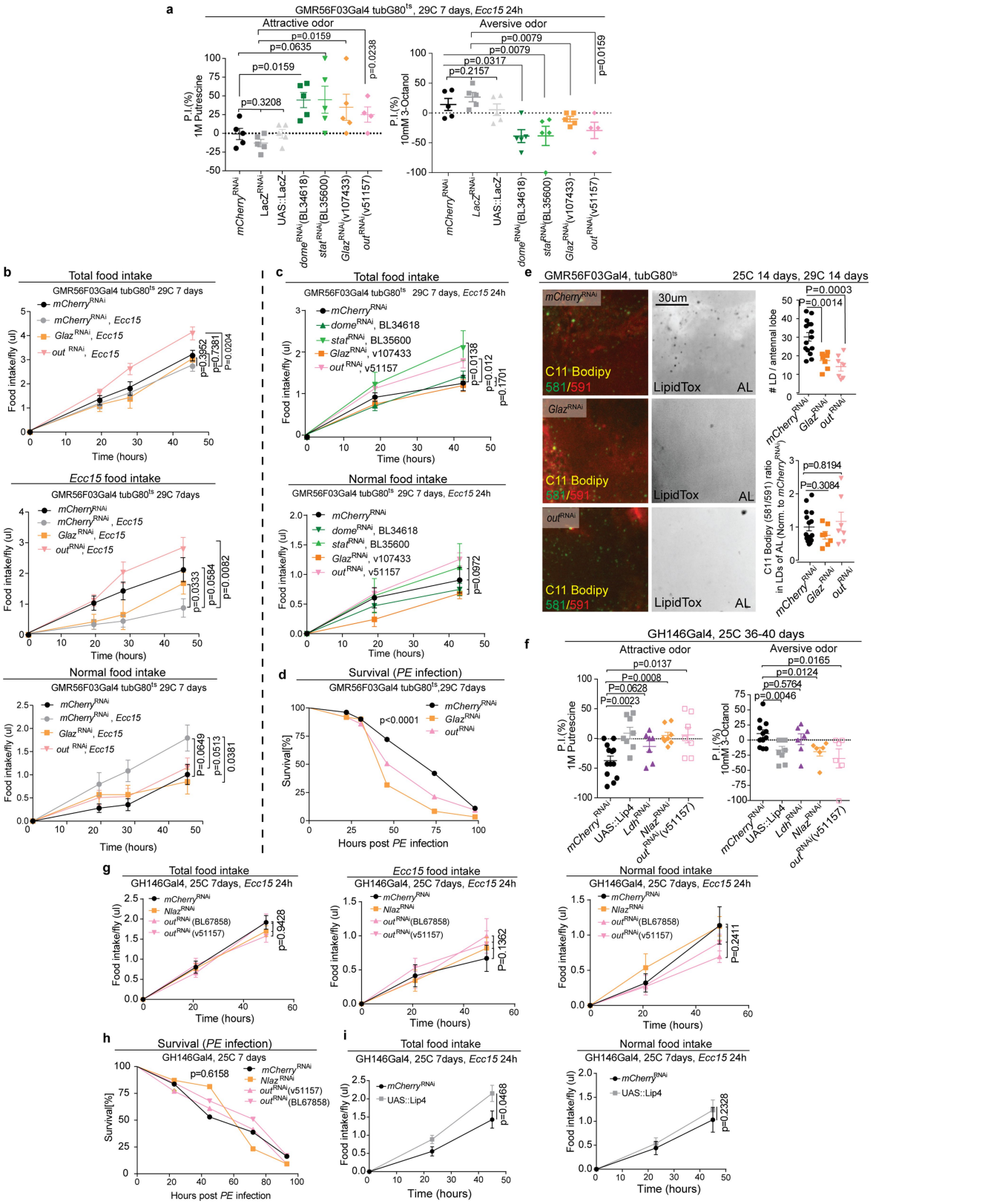

Extended Data Fig. 10 | See next page for caption.

Extended Data Fig. 10 | Inhibiting lipid export or lactate intake in projection neurons partially rescues the decline of olfaction sensitivity upon infection and during ageing. a, Preference index of young infected flies after knockdown of *dome*, *stat*, *GLaz* or *out* in the EG with additional RNAi lines. **b**, **c**, Intake of total food, *Ecc15*$^{+}$ food and normal food for mock flies during homeostasis and for infected flies after the loss of *dome*, *stat*, *GLaz* or *out*, measured by CAFE assay. The *GLaz*^{RNAi} and *out*^{RNAi} lines in **b** and **c** are different. **d**, Survival curve of young flies after loss of *GLaz* or *out* upon continuous *PE* infection. The *GLaz*^{RNAi} and *out*^{RNAi} lines are as in **b**. **e**, Representative images showing LD accumulation and lipid peroxidation at the AL from old flies after knockdown of *GLaz* or *out* in EG driven by GMR56F03::Gal4;tubG80^{ts}. LD numbers per AL were quantified. Lipid peroxidation levels of LDs for each sample were measured as the mean 488/561 nm intensity ratio. The ratios were normalized to the mean value of old control samples. Flies were aged at 25 °C for 14 days followed by 29 °C for 14 days to induce expression of RNAi lines. **f**, Preference index values of old flies overexpressing Lip-4, or knockdown of *NLaz*, *Ldh* or *out* in projection neurons using the GH146::Gal4 driver. **g**, Intake of total food, *Ecc15*$^{+}$ food and normal food for young infected flies after knockdown of *NLaz* or *out* in projection neurons. **h**, Survival curve of flies after knockdown of *NLaz* or *out* in projection neurons upon continuous *PE* infection. **i**, Intake of total food and normal food for young infected flies overexpressing Lip-4 in projection neurons. Data are mean and s.e.m. The sample size is as follows: $n = 5, 5, 5, 5, 5, 5$ and 4 independently performed experiments per condition (from left to right) in **a**, $n = 6, 6, 5$ and 7 replicates (3 flies per cohort) for mock *mCherry*^{RNAi}, *Ecc15 mCherry*^{RNAi}, *Ecc15 GLaz*^{RNAi} and *Ecc15 out*^{RNAi} correspondingly in **b**, $n = 8, 8, 8, 7$ and 6 replicates (3 flies per cohort) for *mCherry*^{RNAi}, *dome*^{RNAi}, *stat*^{RNAi}, *GLaz*^{RNAi} and *out*^{RNAi} correspondingly in **c**, $n = 100$, 59 and 85 flies for *mCherry*^{RNAi}, *GLaz*^{RNAi} and *out*^{RNAi} respectively in **d**, $n = 15, 7$ and 7 brains per condition (from left to right) in **e**, $n = 13, 8, 7, 8$ and 7 independently performed experiments per condition (from left to right) in **f**, $n = 6, 7, 8$ and 7 replicates for *mCherry*^{RNAi}, *NLaz*^{RNAi}, *out*^{RNAi}(v51157) and *out*^{RNAi}(BL67858) correspondingly in **g**, $n = 49, 86, 87$ and 53 flies for *mCherry*^{RNAi}, *NLaz*^{RNAi}, *out*^{RNAi}(v51157) and *out*^{RNAi}(BL67858), respectively, in **h**, $n = 8$ replicates (3 flies per cohort) per condition in **i**. Data in **b**–**d**, **g** and **h** are representative of two independently performed experiments, and those shown in **e** and **i** are representative of three separate experiments. *P* values in **d** and **h** from log-rank test; *P* values in **a** (when comparing *mCherry*^{RNAi}, *LacZ*^{RNAi} and UAS::LacZ), **c** (top: when comparing *mCherry*^{RNAi}, *dome*^{RNAi} and *GLaz*^{RNAi}; bottom) and **g** from Kruskal–Wallis test; other *P* values from two-tailed Mann–Whitney test.

nature research

Corresponding author(s): Heinrich Jasper

Last updated by author(s): Jun 7, 2021

Reporting Summary

Nature Research wishes to improve the reproducibility of the work that we publish. This form provides structure for consistency and transparency in reporting. For further information on Nature Research policies, see our Editorial Policies and the Editorial Policy Checklist.

Statistics

For all statistical analyses, confirm that the following items are present in the figure legend, table legend, main text, or Methods section.

n/a	Confirmed	
☐	☒	The exact sample size (*n*) for each experimental group/condition, given as a discrete number and unit of measurement
☐	☒	A statement on whether measurements were taken from distinct samples or whether the same sample was measured repeatedly
☐	☒	The statistical test(s) used AND whether they are one- or two-sided *Only common tests should be described solely by name; describe more complex techniques in the Methods section.*
☒	☐	A description of all covariates tested
☐	☒	A description of any assumptions or corrections, such as tests of normality and adjustment for multiple comparisons
☐	☒	A full description of the statistical parameters including central tendency (e.g. means) or other basic estimates (e.g. regression coefficient) AND variation (e.g. standard deviation) or associated estimates of uncertainty (e.g. confidence intervals)
☐	☒	For null hypothesis testing, the test statistic (e.g. *F*, *t*, *r*) with confidence intervals, effect sizes, degrees of freedom and *P* value noted *Give P values as exact values whenever suitable.*
☒	☐	For Bayesian analysis, information on the choice of priors and Markov chain Monte Carlo settings
☒	☐	For hierarchical and complex designs, identification of the appropriate level for tests and full reporting of outcomes
☒	☐	Estimates of effect sizes (e.g. Cohen's *d*, Pearson's *r*), indicating how they were calculated

Our web collection on statistics for biologists contains articles on many of the points above.

Software and code

Policy information about availability of computer code

Data collection	No software was used to collect the data in this study.
Data analysis	FlowJo v10; Image J; GraphPad Prism v7.02; Partek Flow; Python (version 2.7); code for scRNAseq analysis is available at Github: https://github.com/Hongjie-Li/flyglia

For manuscripts utilizing custom algorithms or software that are central to the research but not yet described in published literature, software must be made available to editors and reviewers. We strongly encourage code deposition in a community repository (e.g. GitHub). See the Nature Research guidelines for submitting code & software for further information.

Data

Policy information about availability of data

All manuscripts must include a data availability statement. This statement should provide the following information, where applicable:

- Accession codes, unique identifiers, or web links for publicly available datasets
- A list of figures that have associated raw data
- A description of any restrictions on data availability

The authors declare that the data supporting the findings of this study are available within the paper and its supplementary information files. Raw sequencing reads and preprocessed sequence data for Bulk RNAseq files have been deposited in GEO under accession code GSE168530 and scRNAseq reads and preprocessed sequence data have been deposited in GEO under accession code GSE168572. They both are available to the public.
Drosophila genome (version BDGP6) is available for download at https://aug2017.archive.ensembl.org/info/data/ftp/index.html
Drosophila genome (r6.10) is available for download at http://ftp.flybase.net/releases/.
scRNAseq datasets of Drosophila brain during aging published by Dr. Stein Aerts lab are available at https://scope.aertslab.org.

Field-specific reporting

Please select the one below that is the best fit for your research. If you are not sure, read the appropriate sections before making your selection.

☒ Life sciences ☐ Behavioural & social sciences ☐ Ecological, evolutionary & environmental sciences

For a reference copy of the document with all sections, see nature.com/documents/nr-reporting-summary-flat.pdf

Life sciences study design

All studies must disclose on these points even when the disclosure is negative.

Sample size	No statistical methods were used to calculate the sample size. Sample numbers are described in the corresponding figure legends. Sample sizes were determined according to our previous publications and literature in the field, as we are using similar experimental paradigms.
Data exclusions	No data exclusions were done in this study.
Replication	All the experiments were repeated at least twice, as specified in each figure legend.
Randomization	For Ecc15 treatments, flies with the same sex, age and genotype were randomly assigned to control or experimental groups. Where cohorts of animals with defined sex, age and genotypes were compared, animals were randomly collected from breeding cages, sorted according to sex and genotype, and combined into cohorts. As all animals in a cohort were analyzed, no randomization had to be performed in the data collection.
Blinding	To establish cohorts for experiments, the experimenter was not blinded to the genotype, age, or sex of the animals (genotyping and sexing was performed by visual markers, as is standard for Drosophila genetics). Image analysis, quantification, and data analysis were performed on samples that were blinded to the experimenter.

Reporting for specific materials, systems and methods

We require information from authors about some types of materials, experimental systems and methods used in many studies. Here, indicate whether each material, system or method listed is relevant to your study. If you are not sure if a list item applies to your research, read the appropriate section before selecting a response.

Materials & experimental systems

n/a	Involved in the study
☐	☒ Antibodies
☒	☐ Eukaryotic cell lines
☒	☐ Palaeontology and archaeology
☐	☒ Animals and other organisms
☒	☐ Human research participants
☒	☐ Clinical data
☒	☐ Dual use research of concern

Methods

n/a	Involved in the study
☒	☐ ChIP-seq
☐	☒ Flow cytometry
☒	☐ MRI-based neuroimaging

Antibodies

Antibodies used	Primary antibodies and dilution used in this study: mouse anti-repo (DSHB 8D12, 1:100), mouse anti-NC82(DSHB, 1:50-1:100), rabbit anti-GFP(ClonTech, Cat# 632592, 1:500). Fluorescent secondary antibodies were bought from Jackson Immunoresearch (1:500). DAPI was used to stain DNA at 1:1000.
Validation	All the antibodies used in this paper are commercially available. Validation of these antibodies are available at the manufacturer's websites. The RRID and validation reference for each antibody is listed below: 1. mouse anti-repo (DSHB 8D12): AB_528448. https://dshb.biology.uiowa.edu/8D12-anti-Repo 2. Mouse anti-NC82 (DSHB): AB_2314866. https://dshb.biology.uiowa.edu/nc82 3. Rabbit anti-GFP (ClonTech, Cat# 632592): AB_2336883. https://www.labome.com/product/Takara-Bio-Clontech/632592.html

Animals and other organisms

Policy information about studies involving animals; ARRIVE guidelines recommended for reporting animal research

Laboratory animals	For all the studies, we used adult females Drosophila melanogaster. Full genotypes and ages of flies used in each figure are listed in Supplemental Table 1.

Wild animals	No wild animals were used in this study.
Field-collected samples	No field-collected samples were used in this study.
Ethics oversight	This study did not require ethics approval.

Note that full information on the approval of the study protocol must also be provided in the manuscript.

Flow Cytometry

Plots

Confirm that:

☒ The axis labels state the marker and fluorochrome used (e.g. CD4-FITC).

☒ The axis scales are clearly visible. Include numbers along axes only for bottom left plot of group (a 'group' is an analysis of identical markers).

☒ All plots are contour plots with outliers or pseudocolor plots.

☒ A numerical value for number of cells or percentage (with statistics) is provided.

Methodology

Sample preparation	For flow cytometry analysis in Extended Data Fig.2e, 20 brains were dissected for each biological replicate. Single cell suspension of each sample was prepared freshly, using the combination of papain and liberase (Li, et al. 2017. Cell). Cells was stained with eFluor™ 660 on ice (1:1000) on ice. After staining, cells were washed with 1x cold PBS followed by fixation, permeabilization and stainning with anti-GFP antibody (ClonTech, Cat# 632592, 1:500) following a previously published protocol (Cai, et al. 2018.), using eBioscience™ Foxp3/Transcription Factor Staining Buffer Set (ThermoFisher Cat. No. 00–5523–00). DAPI was added to each sample at a final concentration 1µg/mL, to stain nuclei, and analyzed by BD Symphony flow cytometer. Fluorescent secondary antibodies were bought from Jackson Immunoresearch (1:500). For glia live sorting shown in Extended Data Fig.7g, about 100 brains were dissected for each replicate in cold Shields and Sang M3 insect medium (Sigma S8398) containing 10% fetal bovine serum (FBS; ThermoFisher,16000036). Brains were dissociated in the solution containing 300ul papain (Sigma, P4762; dissolved in 1xPBS to a final concentration of 100units/ml) and 4.1ul liberase TM solution (Roche, 5401119001; reconstituted with 1xPBS to a final centration of 2.5mg/ml) at 25°C, 1000rpm for 20min. Cells were stained with Calcein blue (ThermoFisher, c1429, 1:1000) for 20min on ice, washed, and resuspended in dissection buffer with SYTOX™ Deep Red Dead cell stain (ThermoFisher, S11381, 1:1000). GFP+ tdTomato+ cells and GFP- tdTomato+ cells were sorted into Trizol (ThermoFisher, 15596026) respectively with BD FACSAria™ Fusion.
Instrument	BD Symphony flow cytometer; BD FACSAria™ Fusion
Software	FlowJo v10 Software
Cell population abundance	The percentage of GFP+, mCherry+ population among total DAPI+ cells were quantified in Extended Data Fig.2e.
Gating strategy	Gating strategy for Extended Data Fig.2e is illustrated in the same panel with quantifications, as below: Forward versus side scatter (FSC vs SSC); side scatter height vs width (SSC-H vs SSC-W); forward scatter height versus width (FSC-H vs FSC-W); fixable viability dye (eFluor™ 660 to label dead cells before fixation) versus DAPI (labeling nuclei to exclude debris); mCherry versus GFP fluorescence channel (mCherry vs GFP). Gating strategy for Extended Data Fig.7g is illustrated in Supplementary Figure, and is listed as below: Forward versus side scatter (FSC vs SSC); forward scatter height versus width (FSC-H vs FSC-W); side scatter height versus width (SSC-H vs SSC-W); Calcein pacific blue (labelling live cells) versus Sytox APC (labelling dead cells); GFP versus YG-mCherry fluorescence channel.

☒ Tick this box to confirm that a figure exemplifying the gating strategy is provided in the Supplementary Information.